A HIGH-PASS DETUNABLE QUADRATURE BIRDCAGE COIL AT HIGH-FIELD

A Thesis

by

VISHAL VIRENDRA KAMPANI

Submitted to the Office of Graduate Studies of
Texas A&M University
in partial fulfillment of the requirements for the degree of

MASTER OF SCIENCE

May 2008

Major Subject: Biomedical Engineering

A HIGH-PASS DETUNABLE QUADRATURE BIRDCAGE COIL AT HIGH-FIELD

A Thesis

by

VISHAL VIRENDRA KAMPANI

Submitted to the Office of Graduate Studies of
Texas A&M University
in partial fulfillment of the requirements for the degree of

MASTER OF SCIENCE

Approved by:

Chair of Committee,	Steven M. Wright
Committee Members,	Jim X. Ji
	Hsin-I Wu
Head of Department,	Gerard L. Cote

May 2008

Major Subject: Biomedical Engineering

ABSTRACT

A High-Pass Detunable Quadrature Birdcage Coil at High-Field. (May 2008)

Vishal Virendra Kampani, B.S., University of Illinois-Urbana Champaign

Chair of Advisory Committee: Dr. Steven M. Wright

The circuit described in this study is intended for Magnetic Resonance Imaging (MRI) application. The function of this circuit is to transmit RF energy to the sample and then receive the RF energy. The circuit that does this is called a birdcage coil. This coil is capable of producing a very homogenous B1 field over a large volume; it is this aspect of birdcage coils that make them very favorable for animal/human studies as it is necessary that all nuclei in the volume of the coil are excited by uniform RF energy. At high-field (4.7T) when the power is fed to the coil at a single port the coil unable to produce a homogenous B1 field. However when power is fed at multiple ports the performance of the coil improves. In this paper a study is carried out comparing the performance of the coil when power is fed at a single port and two ports. The advantage of feeding at two ports is that there is sqrt(2) improvement in SNR and the RF power efficiency is doubled. In this work strategies are presented for matching, tuning and isolating the two ports. Also, an attempt is made to fabricate a mechanically rigid coil and interfacing the coil with some additional features that will make the coil easy to use. The homogeneity and SNR of a birdcage coil in linear and quadrature mode loaded with saline, oil and CuSO4 phantom was measured on the bench and the scanner. The coil

performance was compared to two other birdcage coils in the lab. It was found that the unshielded trombone coil that was 3 times smaller in volume than the coil presented has 140% higher SNR than the coil presented but the homogenous region of the coil presented is 48% higher than the smaller coil. Lastly on the bench; the SNR of the quadrature coil was 30% higher than the coil in the linear mode.

ACKNOWLEDGEMENTS

I would like to thank Dr. Wright for giving me the opportunity to work in MRSL and my parents for their unequivocal support. Also, I would like to thank all the members of MRSL for their assistance on this project. Lastly, I would like to thank Dr. Charles Saylor (Invivo Inc., Gainesville, FL) for getting me excited about RF coils.

NOMENCLATURE

SNR	Signal-to-Noise Ratio
RF	Radio Frequency
PIN	Positive-Intrinsic-Negative
FDTD	finite-difference-time-domain

TABLE OF CONTENTS

Page

LIST OF FIGURES

FIGURE Page

LIST OF TABLES

1. INTRODUCTION

The first cylindrical birdcage coil was designed and fabricated by Hayes (1). This was a high pass coil which produced a linearly polarized field. On the other hand, a quadrature coil (2) produces a circularly polarized field and is preferred over a linear coil since it improves the SNR by a factor of $\sqrt{2}$ and reduces RF transmission power (3). Specifically, the SNR increases because the noise voltage generated in the two orthogonal modes are not correlated but the signals from the nuclei are correlated. A circularly polarized field implies that the two orthogonal resonant modes are at the same frequency; one mode carries current proportional to sine of the angle around the end loop and the other mode carries current proportional to the cosine of that angle (4). The current distribution in a fabricated linear coil is not the desired sinusoid due to perturbations from asymmetric samples, closely spaced shields and imaging at high-fields (5). Specifically, a saline sample lowers the homogeneity due to RF standing wave and attenuation effects and the closely spaced shield lowers the B1 amplitude (6). These perturbations lead to non-sinusoidal current distribution and consequently B1 field inhomogeneity. The phase of the sinusoidal current distribution can be made uniform by feeding power at multiple locations. In the 4-port design that is presented, the power is input to a single hybrid and then it is delivered to the multiple locations through a second stage of hybrids. Thus, the power that finally reaches the ports has equal amplitude and fixed phase. There are two variations to the 4-port drive both aimed at improving the

---

This thesis follows the style of Concepts in Magnetic Resonance Part B (Magnetic Resonance Engineering).

homogeneity; 1) equal amplitude and variable phase, 2) variable amplitude and variable phase. When a coil is loaded with an octagonal phantom or human head it is necessary to use the equal amplitude and variable phase optimized approach to improve the homogeneity as concluded by the modeling performed by Ibrahim (7). The equal amplitude and phase approach is effective in the study presented as the coil is loaded with a cylindrical phantom. The variable amplitude and variable phase approach is most efficiently implemented with four independent RF sources; complex hardware would probably be required to interface the four sources to the coil. Thus, the 4-port drive presented is not amplitude or phase optimized but is easily implemented using commercially available quad hybrids.

It is possible to improve the homogeneity by driving the coil at 4-ports by using the equal amplitude and fixed phase approach as shown by the modeling performed by Ibrahim (7) Specifically, the birdcage coil was modeled by Ibrahim at 200MHz with a phantom that has electrical properties of muscle tissue and it was concluded that the B1 field homogeneity for the linear and 2-port drive is the same at 29% (the difference between the maximum and the minimum values of the B1 field in the transverse plane is 71% of the maximum value). The lack of improvement in homogeneity from the linear to 2-port drive implies that the 2-port drive was not able to produce a circularly polarized field. A coil is unable to produce the circularly polarized field because the ideal sinusoidal current distribution predicted from circuit analysis is not valid at high frequencies. This is because at high frequencies there is significant interaction between the coil and the object to be imaged. This could be because of the electric field

generated by a conductive sample; this electric field induces currents on the rungs. Additionally, modeling shows that the 29% homogeneity obtained for the linear or 2-port drive improved to 55% for the 4-port drive (7). In other words, the 4-port drive shows a smaller variation in the B1 field compared to the 2-port drive. This improvement is because the 4-port drive basically cancels the modes on either side of the dominant mode and consequently improves the homogeneity. However for a fabricated coil the improvement in homogeneity depends on the method of fine tuning adopted.

In the past researchers have fine tuned birdcage coils by either RF shielding (8) or changing the length of the rungs ("trombone" coil) (9) or a combination of trimmer capacitors (10). The advantage of fine tuning by varying the overlap between the shield and coil or the trombone coil is that it preserves the symmetry of the coil and consequently maintains the sinusoidal current distribution. However, a limitation of tuning by RF shielding is that to maintain optimal B1 magnitude the coils have to be smaller compared to the shield and the shield diameter should be 1.5 times that of the coil diameter (8). Thus this method is useful for tuning small coils for spectroscopy but not for applications (imaging human head) that require a large coil diameter. Furthermore a lack of complete overlap between the shield and the coil defeats the advantage of having a shield. RF shields are helpful in reducing the interaction between the RF coil and the gradient and shim coils. These interactions degrade the performance of the RF coil, like lowering the SNR in MR images. It also provides a stable environment for tuning and matching and improves SNR. At high fields the radiation losses are very high. A shielded coil will make sure that all the energy is within the

cavity of the coil. Thus, it is necessary to completely overlap the shield and coil in applications where coils are close to the shield of the magnet.

Additionally, in this work the 2-port coil was actively detuned with PIN diodes. This was implemented as certain applications require a highly homogenous spatial coverage and high SNR. Both high homogeneity and high SNR can be achieved when the birdcage coil is used for transmit and a localized surface coil is used for receive. Since a birdcage coil can conventionally transmit/receive the birdcage needs to be detuned from its resonant frequency when the surface coil is receiving.

Lastly, researchers have implemented the 4-port drive at low-field for sensitivity-encoded imaging (10) and on TEM coils (11). The 4-port drive for sensitivity-encoded imaging was implemented at 1.5T and the birdcage coil was degeneratively tuned with the dominant mode and the first higher order mode at the resonant frequency. Also, at low field some of the perturbations present at high-field like dielectric resonance and standing waves are absent. Thus, the results from the former study cannot be used to compare the improvement in SNR and homogeneity from linear to 4-port drive at high-field. The results from the 4-port drive implemented on the TEM coil cannot be used to conclude that similar results will hold true for a birdcage coil.

It is the objective of this thesis to present a mechanically rigid 2-port birdcage coil. The coil designer has to choose the dimensions of the coil after taking into consideration the effect on SNR and homogeneity. Next, strategies are presented for tuning, matching and isolating the 2-port drive while keeping the capacitor perturbations to a minimum. Detailed description is given on bench tuning of the coil so that it can be easily be replicated by a novice. Bench measurements are carried out and spin-echo images are taken to evaluate performance of the coil. Lastly, the reader is made aware of various issues faced during the fabrication of this coil and suggestions are given on design improvements for the next generation 2-port birdcage coil.

2. THEORY

2.1 Birdcage Coils

RF coils are used for transmitting RF pulses and for receive. Specifically, the coil generates RF pulses at the Larmor frequency to excite the nuclei in the object to be imaged. When the RF excitation pulse is removed the nuclei will relax; during relaxation the nuclei will emit RF energy at Larmor frequency. This energy will be received by the RF coil. The birdcage coil is a volume coil and is an example of a RF coil. Surface coils are also an example of RF coils. Volume coils are preferred over surface coils because volume coils have a bigger field of view as compared to surface coils and thus volume coils are able to produce a homogenous B1 field in the volume of interest so that the nuclei can be uniformly excited. Surface coils have the advantage that they are small and can be made of various shapes to fit the contour of the object tot be imaged. So the SNR of the surface coil will be higher than the volume coil, since the surface coil is in close proximity to the sample. But, the disadvantage of surface coils is that the sensitivity falls off quickly. In other words, surface coils have a low penetration depth as compared to volume coils.

The birdcage coil is made of multiple parallel conductive segments that are parallel to the z axis. These parallel conductive segments are referred to as the rungs. These rungs interconnect a pair of conductive loop segments. A high-pass coil is where the conductive loops have capacitors between adjacent rungs (inductor). A low-pass coil is where the capacitors at the mid-point of the rungs; the conductive loop in this case are inductors. They are situated at the center of rung because the voltage at the center of

rungs is zero. A hybrid coil is where the capacitors are located on the loop segments and the rungs. A high-pass is so called as the high frequency signals will tend to pass through capacitive elements in the conductive loops because at high frequency the capacitors will present low impedance compared to inductors, which will give high impedance. Conversely, low frequency signals will be blocked by capacitive elements that will give high impedance and shorted by inductive elements as they will give low impedance. The same argument applies to low-pass coil.

The meshes repeats N (where N is the number of legs) times. The end ring segments of the two conducting loops are represented by inductors and capacitors. The adjoining meshes to the feed point ($I_{j+!,}$ I_{j-1}) are mutually inductively coupled (M_{j+1}, M_{j-1}) to the feed mesh. When the coil is fed at a particular location it creates N/2+1 resonant modes; where N is the number of legs. The meshes that are orthogonal to each other produce orthogonal resonant modes that are degenerate and hence the number of modes created are N/2 and not N.

Applying Kirchhoff's voltage law to the mesh structures shows that , we get

$$-iwM(I_j - I_{j-1}) - iwM(I_j - I_{j+1}) - 2iwLI_j + \frac{2i}{wC}I_j = 0 \quad \text{where (j=1,2,…N)} \qquad [2.1]$$

The above equation can be re-written as

$$M(I_{j+1} + I_{j-1}) + 2(\frac{1}{w^2C} - L - M)I_j = 0 \qquad [2.2]$$

Because of cylindrical symmetry, the current I_j must satisfy the periodic condition I_{j+N} $=I_{j.}$ Therefore, the N linearly independent solutions (or modes) have the form

$$(I_j)_m = \cos\frac{2\pi mj}{N} \qquad m = 0,1,2,...,\frac{N}{2} \qquad [2.3]$$

$$= \sin\frac{2\pi mj}{N} \qquad m = 0,1,2,...,\frac{N}{2}-1$$

Where $(I_j)_m$ denotes the value of I_j in the mth solution. The current in the jth leg is then given by

$$(I_j)_m - (I_{j-1})_m = \begin{cases} -2\sin\frac{\pi m}{N}\sin\frac{2\pi m(j-\frac{1}{2})}{N}; m = 0,1,2,...,\frac{N}{2} \\ 2\sin\frac{\pi m}{N}\cos\frac{2\pi m(j-\frac{1}{2})}{N}; m = 0,1,2,...,\frac{N}{2}-1 \end{cases} \qquad [2.4]$$

To find the resonant frequencies or modes substitute equations 2.3 into equation 2.1 and we get

$$w_m = [C(L + 2M\sin^2\frac{\pi m}{N})]^{-1/2} \qquad m = 0,1,2,...\frac{N}{2} \qquad [2.5]$$

In this equation m=0 gives the end-ring mode and m=1 gives the dominant mode.

It was shown by Hayes that when the cumulative phase shift around the loops equals 2*pi a standing wave resonance is created. The mode when the coil has a standing wave is called the dominant mode. The current in the legs approximate a sinusoidal current distribution sin θ at the resonant frequency . The higher order modes have a null at the center and are created when the cumulative phase shift around the network equals 4*pi radians; the current in the wire is proportional to sin 2π . It can be shown that when there is a z-directed surface current on the coil legs then it creates an increasingly homogenous field in the transverse plane.

Depending upon the method of feed to the coil the polarization produced is linear or circularly polarized. Its linear when the B field produced is either x or y axis. A circularly polarized field is B field along x and y axis. Specifically, when the coil is fed along y axis the B field is proportional to;

$$B1 = \hat{x}B_0 * \cos(wt) = B_{CW} + B_{CCW} \quad [2.6]$$

Where,

$$B_{CW} = \frac{1}{2}B_0(\hat{x}\cos wt - \hat{y}\sin wt)$$
$$B_{CCW} = \frac{1}{2}B_0(\hat{x}\cos wt + \hat{y}\sin wt) \quad [2.7]$$

The B1 field can be broken down into the CW component and CCW component. The two fields are rotating in opposite direction in the transverse plane perpendicular to the direction of B_0 field. The nuclei responds to only one of the two rotating fields. Hence the power used to create the field rotating in the wrong direction is wasted. If the B1 field oscillates at the same frequency with which the rotating frame oscillates then

$$B_{CW} = \frac{1}{2}B_0\hat{x}_1$$
$$B_{CCW} = \frac{1}{2}B_0(\hat{x}_1\cos(2w_r t) + \hat{y}_1\sin(2w_r t)) \quad [2.8]$$

Where,

$$\hat{x}_1 = \hat{x}\cos w_r t - \hat{y}\sin w_r t$$

$$\hat{y}_1 = \hat{x}\sin w_r t + \hat{y}\cos w_r t$$

Thus, from eq. 2.8 we can see that half of the supplied power is wasted. Whereas, when the coil is fed at two locations a circularly polarized field (either CCW or CW) is produced that rotates in the same direction as the nuclei. Hence all the energy supplied to the coil is absorbed by the nuclei. So, the 2-port drive doubles the RF power efficiency.

2.2 SNR Improvement due to Quadrature Detection

Various authors have mentioned that there is sqrt(2) improvement in SNR when signals are detected from 2 locations that are 90degrees apart. In this section I will explain where this improvement in SNR comes from.

When the intensity of the signal sent from one coil is equal to that of the signal sent from the other coil perpendicularly intersecting the first coil, the sensitivity is ideally improved by sqrt(2) as compared with the detection of the single signal (12). Thus, the outputs of the quadrature coils are combined so as to increase the strength of the received signal according to the simple sum of the output signals from the coils. The strength of the noise component of these signals however will increase only according to the square root of the sum of squares of the uncorrelated coil components. Doing the above will give an approximate gain of sqrt(2) due to the lack of inductive coupling between the coil pairs. This ensures that only the uncorrelated noise components add. In the presence of inductive coupling the correlated and uncorrelated noise components will add thus effectively reducing the effective SNR ratio (13).

Specifically, consider two coils with the signal voltage in coil 1 is V1 and the noise voltage N1. Similarly, the signal voltage in coil 2 is V2 and the noise voltage is N2 in coil 2. The individual SNR values are then (14) ;

$$\text{SNR1}=\frac{|V1|}{\sqrt{\left\langle |N1|^2 \right\rangle}} \quad \text{and SNR2}=\frac{|V2|}{\sqrt{\left\langle |N2|^2 \right\rangle}} \qquad [2.9]$$

The combination SNR for two orthogonal coils that are put through a quad hybrid is (14);

$$\text{SNR}=\frac{|V1+j*V2|}{\sqrt{\left\langle |N1+j*N2|^2 \right\rangle}} \qquad [2.10]$$

The above equation can be used to show the sqrt(2) improvement on using the quadrature drive compared to the linear drive.

A derivation can be made that shows the sqrt(2) improvement in SNR by considering the polarization vector too.

$$B_t = \bar{B}1.\hat{p} \qquad [2.11]$$

For the above equation for the linear feed:

$$B_{linear} = \frac{B1}{2}\hat{a}_x \bullet (\frac{\hat{a}_x + j\hat{a}_y}{\sqrt{2}}) = \frac{B1}{2\sqrt{2}} \qquad [2.12]$$

$$B_{c.p} = (B1\hat{a}_x) \bullet (\frac{\hat{a}_x + j\hat{a}_y}{\sqrt{2}}) = \frac{B1}{\sqrt{2}}$$

In the equation of 2.12 the polarization of the transmit signal is CCW but the polarization of the receive signal is CW. Thus, the negative sign. Next, to show the improvement in SNR the equation used by Wright (15) can be used;

$$SNR = \frac{B_t}{\sqrt{R_{coil}}} \quad [2.13]$$

For the quadrature mode the noise is uncorrelated and it is equal as both meshes are matched to 50ohms.

$$N_l = \sqrt{R_{coil}} = \sqrt{50}$$
$$N_{c.p} = \sqrt{R_{coil1} + R_{coil2}} = \sqrt{50+50} = \sqrt{100}$$

$$\frac{N_{c.p}}{N_l} = \sqrt{\frac{100}{50}} = \sqrt{2}$$

Thus, SNR for linear and quadrature is

$$SNR_l = \frac{B1}{N1 * 2\sqrt{2}} \quad [2.14]$$

$$SNR_{c.p} = \frac{B1}{N1 * 2}$$

Thus, dividing equation 2.14 we see the sqrt(2) improvement;

$$\frac{SNR_{c.p}}{SNR_{linear}} = \sqrt{2} \quad [2.15]$$
$$\therefore SNR_{c.p} = \sqrt{2} * SNR_{lineat}$$

In conclusion, the signal increases by a factor of 2 from linear to quadrature and the noise increases by a factor of sqrt(2) from linear to quadrature.

2.3 Correction Capacitors for 2-port Feed

The Discussion section of the thesis talks in detail about the various sources that made the coil presented in this thesis asymmetric. Briefly, for a 2-port feed it is important that the two orthogonal modes of the coil are at the same resonant frequency. However, due

to fabrication errors in the coil the two orthogonal modes are rarely at the same frequency. The following section presents some equations that can be used to determine the capacitance and location of the correction capacitors to make the 2-port coil symmetric. Also, the price paid in adding these symmetric capacitors is that there will be a drop in SNR of the coil. These equations and the accompanying commentary can be found in Tropp (16). There will be cross-talk between the two ports of an asymmetric coil when the two feed meshes are not exactly mechanically aligned (coupling by mutual inductance) or there is substantial stray E field interaction between the two feed meshes (coupling by mutual capacitance). In terms of circuit theory this coupling can be characterized by mutual impedance between the two meshes. The correction capacitors need to be added at 45^o azimuthal separation and should be placed parallel to the end-ring capacitors. The location of the correction capacitor is on the end-ring close to the rung where the largest current goes through. The magnitude of the correction capacitor C is;

$$C = C_o[\frac{\delta}{1-\delta}] \qquad [2.16]$$

Where, C_o is the end ring capacitance and $\delta = \frac{N * \Delta}{w_o}$ and N is the number of rungs in the ladder, Δ is the numerical difference between the maximum and minimum frequencies due to the splitting of the resonant frequency caused by mutual impedance between the two meshes.

The loss in SNR when the two meshes of the coil are not orthogonal (not perfectly isolated);

SNR loss=-10*log (1+η^2) [2.17]

Where η is normalized coefficient of coupling and is defined as $\eta = Q * \xi$

Where, Q is the quality factor of the birdcage coil and ξ is the coefficient of coupling defined $\frac{\delta w}{w_o}$, δw is the separation of resonance frequencies and w_O is the undisturbed frequency.

In practice, to solve the problem of asymmetry I randomly picked a capacitor and tried all 14 end ring locations. For 2-port to work the modes have to be on the same frequency thus the loss in SNR is something that is unavoidable. The Discussion section talks about ways to make the coil as symmetric as possible so that less correction capacitance is required and thus loss in SNR will be lower.

2.4 Loaded Q of Circuit

The Quality factor of circuit is defined as;

Q= 2π *maximum energy stored/ total energy dissipated per period

$$Q = \frac{w_r}{\Delta w} \quad [2.18]$$

A coil designer would like to have the unloaded and loaded Q has high as possible as a high numerical Q translates to more energy being stored in the sample/coil space. Generally, an unloaded Q of 100, loaded Q of 20 is considered good. Thus, a ratio of unloaded Q to loaded Q is 5. Also, we would like to have the ratio of unloaded to loaded Q as high as possible. Sample loading degrades Q because currents induced by axial RF magnetic fields and electric fields from self inductance of the coil.

However, to accurately find out the amount of energy stored in the sample, we would like to calculate the magnetic filling factor (5). Filling factor (η) is defined as the magnetic energy in the transverse component of the magnetic field throughout the sample divided by the total magnetic energy ($T=I^2L/2$ for a simple RF coil with inductance L and current passing through it is I) throughout all space.

$$\eta = \frac{\int_s B_1^2 dV}{2*\mu_0 * T} \qquad [2.19]$$

2.5 Effect of Shield

In the Introduction section the advantages of having a shield were mentioned. It was said that the shield blocks RF waves but allows the gradients to go through. By image theory, it can be shown that z directed currents are produced on the shield that is equidistant and in a direction opposite of the current flowing on the rungs. Thus, the shield satisfies the boundary condition. However, the presence of shield will lowers the SNR and having a coil closely spaced to the shield further degrades the SNR. Firstly, the shield lowers the SNR because of resistance offered by the copper conductor. This shield resistance increases as the frequency is increased because of skin effect. Thus a shield with lower dissipation factor should be used. The following equation shows the power dissipated in the shield and its relation to SNR;

$P_{shield} = R_{Cu} * \oint_{shield} |J_s|^2 .dl$; Js is the surface current density on the shield

$$R_{shield} = 2 * \frac{P_{shield}}{I} \qquad [2.20]$$

$$SNR\alpha\frac{B_1}{\sqrt{R}} \qquad [2.21]$$

Where, R=Rsample+ Rsheild+ Rlegs

Js is the surface current density on the shied

Furthermore, the closely spaced shield it has been experimentally shown by Doty (5) at high-field that the magnetic filling factor decrease but the loaded Q increases. The following relation between SNR, filling factor and loaded Q was used by Doty to show the drop in SNR;

$$\text{SNR } \alpha(\eta_f * Q_L)^{1/2} \qquad [2.22]$$

In particular the effect of closely spaced shield can be shown using the data obtained by Doty for the two coils that were fabricated; for the shield diameter of 20cm, coil diameter of 10cm, sample diameter is 8cm and sample length is 8cm, measured unloaded Q was 268 and loaded Q was 13, filling factor was 13.2 and inhomogeneity was 5%. Next, shield diameter of 12cm, coil diameter of 10cm, sample diameter of 8cm and sample length of 8cm, measured unloaded Q was 165 and loaded Q was 29, filling factor was 4.4 and inhomogeneity was 13%.

2.6 Effect of Imaging with Higher Permittivity and Higher Conductivity

As mentioned earlier the SNR will be degraded because of the resistance offered by the sample along with that the homogeneity in large samples will also be lower. The homogeneity is lower because the sample has a conductivity (σ) and permittivity (ε) that is higher than that of air. The effect of higher conductivity is that eddy currents are induced in the subject by the applied RF magnetic field, and these eddy currents in turn

produce an RF magnetic field which adds to that produced by RF coil. The result is a nonhomogeneous RF field in which the field strength varies as a function of distance around the central axis. As a result, images are produced in which bright areas appear in two quadrants and dark areas appear in other two quadrants. It is said that a circularly polarized field can fix inhomogeneities caused by eddy currents. Specifically, the variable δ is defined as the depth at which the RF field amplitude is reduced to 1/e (37%) of its initial value for a plane wave impinging on a planar boundary:

$$\delta = \sqrt{\frac{2}{\mu * w * \sigma}} \qquad [2.23]$$

The above equation shows that as conductivity (σ) is increased the depth at which the RF signal drops to 37% is lower.

Additionally, the homogeneity is lowered because of higher permittivity. This is a significant cause of distortion in the images shown below. As the air permittivity is 1 and the permittivity of the sample used is 75. The wavelength of the RF field is shortened in the sample and this produces a standing wave in which the field strength varies as a function of radial distance. The standing wave cycles between peaks and valleys as a function of radial distance from the central axis, and the resulting image has a series of dark and bright rings. The following equation relates the wavelength in a sample to the permittivity of the sample at a given frequency;

$$\lambda = \frac{1}{f\sqrt{\varepsilon * \mu}} \qquad [2.24]$$

For instance, at 200MHz with relative permittivity of 75, ε_0 of 8.85*10^(-12) and μ of 4*pi*10^(-7) ; the wavelength is 17cm.

2.7 Losses at High-field

Building large volume RF coils at high-field is a challenge because the SNR depends on a variety of issues. It is common knowledge that we would like to image at high-field because as the frequency due to the static field increases the SNR increases. However there are losses that come along with increasing the frequency that the coil designer has to be aware of. In theory large coils are those that are longer than $\lambda/10$, these long coils are largely inductive. Specifically, at 200MHz the λ in air is 150cm; $\lambda/10$ is 15cm. The length of the coil presented is 20cm. Thus, it is large. These large coild begin to radiate a large portion of their energy as an antenna. These radiation losses subtract energy from the RF coil's B1 field and add energy as heat and noise signal to the subject and the bore. Thus, to reduce these radiation losses a RF shield is necessary.

The following equation relates SNR to a variety of losses. All these losses have a frequency dependence too as can be seen from the equation;

$$SNR\alpha \frac{w^2 * B1}{\sqrt{R_\Omega + R_r + R_{tissue}}} \qquad [2.25]$$

Where; R_Ω,, R_r , R_{tissue} are the coil's ohmic resistance, radiation resistance and coupled tissue losses, respectively.

Specifically, losses to the tissue conductor are proportional to w. Losses to the tissue dielectric are proportional to w^2. Additionally, the resistive loss of the coil increases as $\sqrt{w}$.

$$R_{\Omega} = \sqrt{\frac{w * \mu}{2 * \sigma}} * \left(\frac{l}{a}\right) \quad [2.26]$$

where l is the length of the coil and a is the width of the coil.

Lastly, radiation losses increase as w^4. In the equation below S is the area bounded by a unit cross-section of the coil.

$$R_r \alpha S^2 * w^4 \quad [2.27]$$

2.8 Voltage Detected by a Crossed-probe

Figure 1 Crossed-probe used to measure the two orthogonal resonant modes. A description of the voltage detected by this probe is given in this section.

The effectiveness of the RF coil in producing a quadrature field can be verified by using a crossed-probe (see Fig. 1). Specifically, when either the input to the hybrid (analyzer/ 50ohms cables) or the two crossed-probe terminals connecting the hybrid are

switched then in one configuration a quadrature field is generated and in the other configuration there is no received signal (reverse polarization). This section educates the reader on the math behind a quadrature field being generated in one configuration and no signal in the other configuration.

The crossed-probe can be connected to the two terminals of the quad hybrid and the signal at the output port can be detected by the analyzer via a S21 measurement.

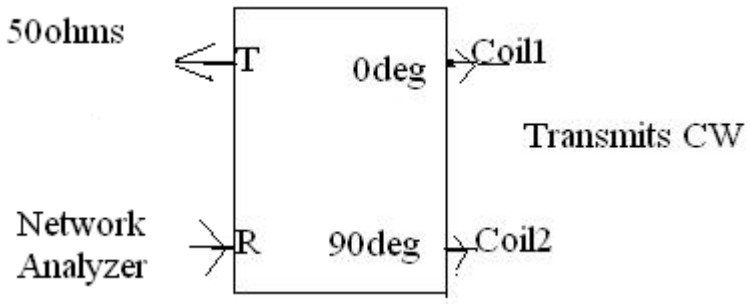

Figure 2 Configuration of transmit quad hybrid. The above configuration either produces a CW or a CCW field. For illustration purposes the above configuration produces a CW field.

The power input at port R is split equally and the two outputs of the quad hybrid are out of phase by 90degrees. The two outputs are then fed to the coil (see Fig. 2). This produces a current on the rungs that is proportional to the cosine and sine. The magnetic field produced by the combination of sine and cosine current is circularly polarized. The quad hybrid on the transmit side produces either a CCW field (equation 2.28) or CW field (equation 2.29)

$$\overline{B} = B\cos wt\hat{x} + B\sin wt\hat{y} \qquad [2.28]$$

$$\overline{B} = B\sin wt\hat{x} + B\cos wt\hat{y} \qquad [2.29]$$

Let us assume that the field produced by the transmit hybrid is CCW.

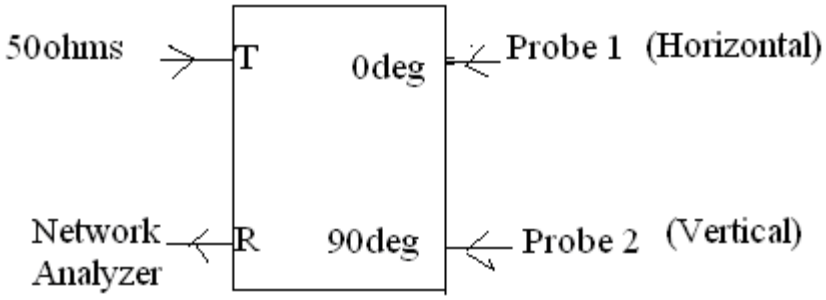

Figure 3 The quad hybrid on receive. The two terminals (Horizontal and vertical) of the crossed-probe are connected to the hybrid.

Again, the CCW field produced by the transmit quadrature birdcage coil is given by equation 2.29.

Flux induced in probe 1 (horizontal) due to a CCW B1 field (see Fig. 3)

$\Psi 1 = B*\cos wt*C$ [2.30]

Where, C is the area of the horizontal loop.

EMF generated in horizontal loop=EMF1= $\frac{d\Psi 1}{dt} = -B*C*\sin(wt)$ [2.31]

EMF generated in vertical loop=EMF2= $\frac{d\Psi 2}{dt} = B*C*\cos(wt)$ [2.32]

EMF1 and EMF2 passes through quad hybrid on receive side and add in amplitude and the phase of EMF2 is delayed by 90degrees and phase of EMF1 is the same**.**

Thus, signal received at "R" =EMF1+EMF2=-B*C*sinwt + B*C*cos(wt-90)

=-B*C*sin(wt)+B*C*sin(wt)

=0 [2.33]

(assuming both horizontal and vertical loops are same area)

When**,** EMF1 is delayed by 90degrees and EMF2 is the same;

signal received at "R" =EMF1+EMF2=-B*C*sin(wt-90) + B*C*cos(wt)

=B*C*cos(wt)+B*C*cos(wt)

=2*B*C*cos(wt) [2.34]

(assuming both horizontal and vertical loops are same area)

In conclusion, the transmit birdcage coil produces a CCW field. It is important that the crossed-probe terminals be connected to hybrid so that it also detects a CCW field on the bench. (As can be seen from eq. 2.33 and eq. 2.34)

Alternate way of looking at it is instead of switching the crossed-probe input to the hybrid, the port "T" and port "R" on the receive hybrid can be switched between the network analyzer (S21) and 50ohms load. One of the two configurations will give a signal and the other will give no signal. (see Fig. 4)

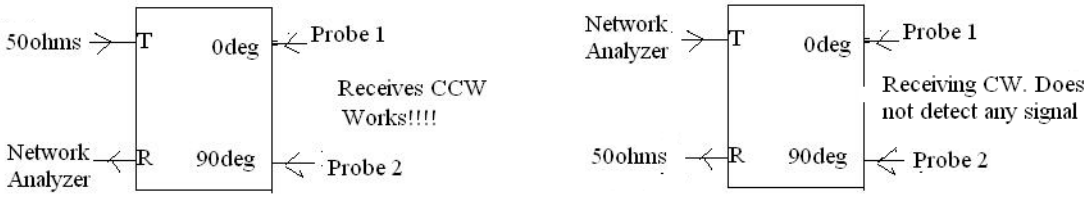

Figure 4 The crossed-probe inputs to the hybrid are not switched. However, the network analyzer and the 50ohms load are switched. In, one of the configurations we will detect a CCW field and the other configuration a CW field.

On a separate note on the bench; a CCW field is transmitted and a CCW field is received. However, in the magnet during imaging a CCW field is transmitted and a CW

field is received. This is because during receive the nuclei of the sample rotates in the opposite sense compared to transmit.

2.9 4-port Theory

In the Introduction section of this thesis some of the advantages of using a 4-port drive were described. The two main advantages are it improves the homogeneity of the dominant mode and reduces the size of the RF amplifiers. The following commentary is reproduced from Bridges (17). For certain coil designs it is possible that the coil has a low Q. In this case, the coupling between the drive loop and the RF coil may change and so that the magnetic field of the desired mode is not completely uniform. Also, for a low Q coil it is possible that the higher modes begin to overlap with the dominant mode and thus the homogeneity of the coil is reduced. To overcome these disadvantages the coil is fed 180^{o} away from each of the orthogonal imaging modes. When the coil is driven in this "push-pull" fashion the modes higher and lower to the dominant mode are cancelled. Specifically, for the high-pass coil the end ring mode and the higher order mode are cancelled. The modes cancel because only the dominant mode has a sinusoidal current distribution of 2*pi. When the coil is fed at two locations spatially separated by 180^{o} with a current that is 180^{o} out of phase; the phase of the current is correct for the dominant mode but is not correct for the end ring and higher order modes. Thus the dominant mode is unaffected but the other modes cancel.

2.10 Planar Pair vs. Rectangular Loop

To accurately measure the current distribution on the legs of the birdcage coil we decide to use a planar pair coil. This is because the sensitivity profile of a planar pair coil is

narrower compared to the profile of a rectangular loop. We would like the profile to be narrow as the rungs are closely spaced at 3cm away from each other. It was reported by McDougall (18) that the coupling coefficient was four times greater at the distance corresponding to the “nearest neighbor distance” for the loop coils compared to the planar pair. Therefore, the planar pair coils were used to measure the current distribution on the rungs.

3. MATERIALS AND METHODS

3.1 Coil Construction

The birdcage coil was fabricated using hollow copper tubes (McMaster Carr, 7190K54) and circular end rings machined from a FR-4 sheet (dielectric constant of 4.35 and thickness 0.16cm). Copper tape can also be used instead of FR-4 end rings and copper tubes. In this design, each rung is made by a combination of two tubes that are about the same diameter. One of the tubes is slightly smaller than the other tube so that they can be inserted into one another. This was done to bring the self-resonant frequency of the coil as close to the desired resonant frequency (200.228MHz) without having to change all 32 end ring capacitors. The end rings were designed to have 16 holes and 16 gaps to accommodate the tubes and capacitors (ATC 100B) respectively (see Fig. 5). These end rings were mechanically etched in Magnetic Resonance Systems Lab using a C30 PC board prototyper. Furthermore, the shield was made by wrapping a sheet of Pyralux (Dupont, AC182500R) on the acrylic former.

Figure 5 The top and bottom end-rings and the 16 Cu tubes that make the rungs. The length of the coil/length of the rungs was 20cm.

Figure 6(a) Dupont pyrulax shield wrapped on the acrylic former.

Figure 6 (b) Tuning sticks with dials. The top picture shows the Pyurilac shield that is wrapped around a 19.4cm former. The bottom picture shows the dials that is mounted at the end of tuning sticks. The dial is to keep track of the position of the variable capacitors.

Lastly, the phantom was made of 41.1mM NaCl, 14.2mM $NiCl_2.6H_20$ and 1.1L of deionized water (19). There were 2 phantoms made with the same constitution; the first phantom had a hole (2cm diameter) this was done to accommodate the pick-up probe for bench measurements, the second phantom was a complete cylinder to be used for imaging. The specific conductivity of this phantom is 0.4 S/m (5). A saline solution was chosen as it mimics the physiological constitution of animals.

The dimensions of the phantom, coil and shield former are given in Table 1. The chosen shield dimension (see Fig. 6(a) & (b)) was commercially available and is the biggest that would fit in the gradient coil (I.D=19.5cm). The dimension of the phantom was chosen after taking into consideration the homogenous B0 field of the magnet and the homogeneous region of the B1 field in an unloaded linear coil. After the shield and phantom diameter are fixed- the coil dimension can be optimized for either homogeneity or SNR. If the coil is closely spaced to the shield then there is an improvement in

homogeneity but a drop in coil SNR. Similarly, if the coil is slightly larger than the phantom then the coil has a higher SNR but poor coil homogeneity (20). In this study, we wanted the coil to be further away from the sample so that we can have higher B1 field homogeneity and thus the coil was placed close to the shield. Specifically, in the design presented the sampling volume fills 48% of the coil volume and the ratio of the shield diameter to coil diameter is 1.2.

Table 1 Dimensions of the birdcage coil

	Material	Inner Diameter (cm)	Outer Diameter (cm)	Length (cm)	Manufacture	Part #
End ring	FR-4	15.30	17.40	None	LPKF (in-house)	none
Rod/Rung	Copper	0.25	0.31	20	McMaster Carr	7190K54
Coil	Acrylic	14.60	15.24	150	US Plastics Corporation	44550
Shield	Acrylic	18.66	19.30	40	US Plastics Corporation	45984
Phantom	PVC	9.52	10.16	12	US Plastics Corporation	29011

3.2 Optimal Birdcage Coil

As mentioned previously once the phantom and shield diameter are fixed, the diameter and length of the rungs of the birdcage coil can be optimized either for SNR or homogeneity. In the following section; a brief description is given on the modeled coil, the method used to find the dominant mode and the SNR and homogeneity of a 12.7cm coil and a 14.6cm coil.

A model of the coil, shield and phantom was created in XFDTD. This software was chosen because of its simple user-interface. Specifically, the length of the 16 rungs was 12cm, the diameter of the cylindrical shield was 17.8cm, length of the shield was 40cm, diameter of phantom was 13cm, dielectric constant and specific conductivity of the phantom was 80 and 0.3 respectively. The electrical parameters of the sample used for modeling were similar to that used for actual imaging. The sample used on the bench for imaging had a dielectric constant of 75 and conductivity of 0.3. The coil diameter was varied between 12.7cm and 14.6cm. The choice of the coil diameter was constrained between 12.7cm and 14.6cm, as the lab already had two working coils of dimension 12.7cm and 14.6cm in diameter. It was necessary for the birdcage coil to be atleast 12.7cm as the intended application was to use the birdcage coil as transmit and use the surface coil (diameter is 13cm) as receive.

An important consideration when specifying the grid size and number of ports used to excite the coil is the time taken by the software to generate a frequency spectrum and time domain B1 field distribution. The grid size of the coil model described by Ibrahim (6) was 3mm and the coil was excited at 2 ports, whereas the model described by Collins (21) the grid was 2mm and the coil was excited at 32 locations. The grid size chosen for this study was 4mm and the coil was excited by a differentiated Gaussian pulse at 32 ports. The pulse with equal amplitude and the appropriate phase (i.e. phase was assigned with respect to its spatial location) was placed across each of the capacitors in the top and bottom end ring. This was done to speed-up the execution time to generate the frequency spectrum. For instance, if the coil is excited at 32 places then

the time taken to generate the frequency spectrum is 30minutes. But when the coil is generated at 4 locations the time taken is 120 minutes. Thus, exciting at 32 ports is faster by a factor of 4 compared to excitation at 4 ports. The spectrum shows only one mode and this is the dominant mode as a sinusoidal distribution is being enforced on the top and bottom end ring (see Fig. 7 (a) & (b)). If the dominant mode is not at resonant frequency (200MHz) then all 32 capacitors are changed and the frequency spectrum is again generated. It was found that 47pF brings the dominant mode to resonant frequency. Once the dominant mode is at resonant frequency a time domain voltage source is placed at 4 ports on the top end ring. Again, to speed-up the execution time the coil was excited at 4 ports instead of just a single port.

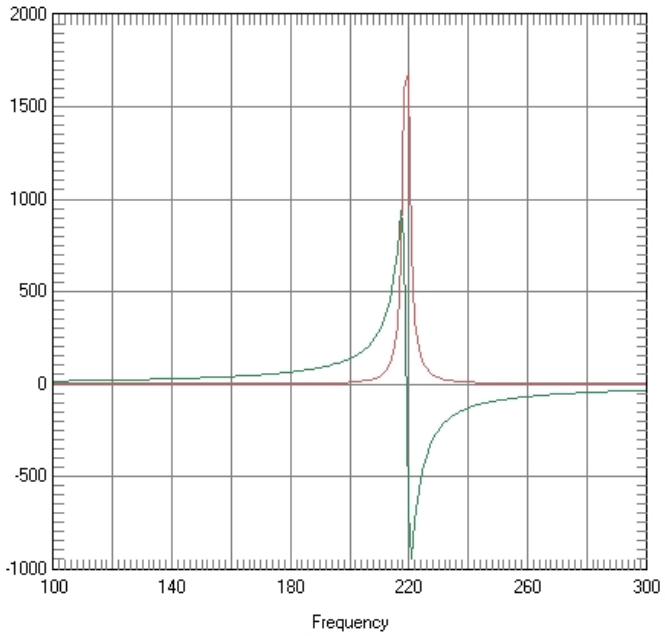

Figure 7(a) Only the dominant mode of the modeled birdcage coil in FDTD. The Gaussian pulse with equal amplitude and appropriate phase was used to excite each of the 32 capacitors in the top and bottom end rings.

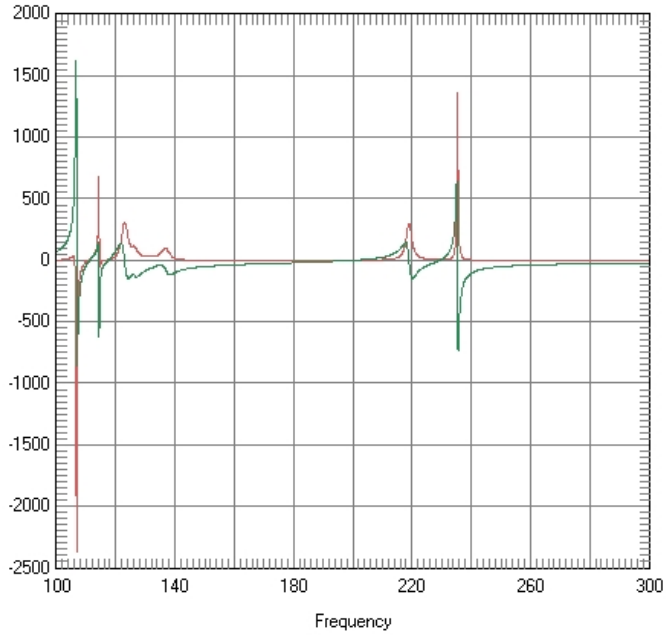

Figure 7(b) All the modes of the modeled birdcage coil. The coil is excited only at one location on the top end ring.

The FDTD software gives the option of displaying B1 values for $\sqrt{(B_x^2 + B_y^2)}$. These values were used to calculate the SNR and homogeneity. The SNR was calculated by averaging the values from random points (10 points) within a rectangle in the central transverse plane. The homogeneous region is defined as the region where the $\sqrt{(B_x^2 + B_y^2)}$ values are within 10% of the central maximum value. In order to compare the performance of coils with different diameters, the SNR and homogeneity are multiplied by appropriate weighting coefficients and then added.

The two coil diameters that were modeled where 14.6cm and 12.7cm. In order to speed-up the execution time the coil was excited at 4 ports. Fig. 8 shows the B1 field distribution for the coil loaded with the phantom but without the shield. The average

SNR in the central transverse plane was 4.9 calculated by taking 10 random points in that plane. The homogenous region along either the x or y axis was 10.4cm. Fig. 9 shows the B1 field distribution along the y axis for the 14.6cm coil with a shield and loaded with a phantom. The average SNR in the central transverse plane was 2.75 calculated by taking 10 random points in that plane. The homogenous region along either the x or y axis was 4.4cm. Fig. 10 shows the B1 field distribution along the y axis for the 12.7cm coil with a shield and loaded with a phantom. The average SNR in the central transverse plane was 4.1 calculated by taking 10 random points in that plane. The homogenous region along either the x or y axis was 4.4cm too.

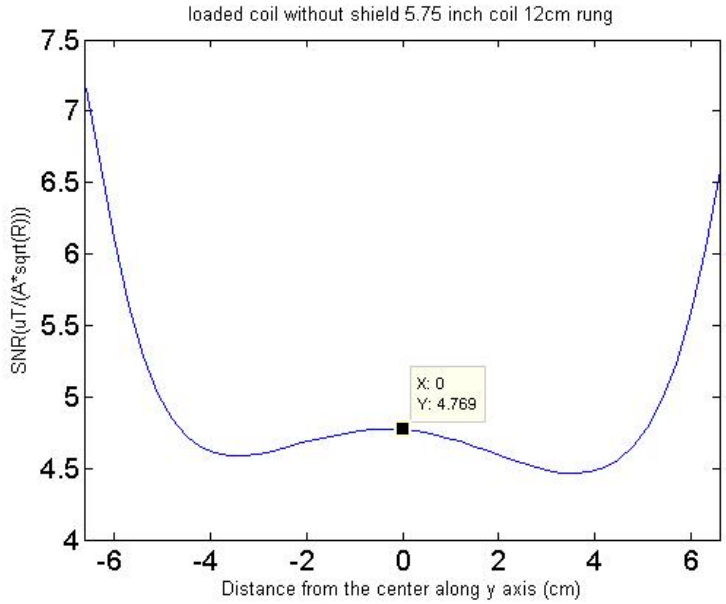

Figure 8 Homogeneity along y axis for a 14.6cm coil without shield but loaded with a phantom. The small variation in amplitude of B1 agrees with the theoretical operation of a birdcage (i.e. the region in the central transverse plane should show little variation)

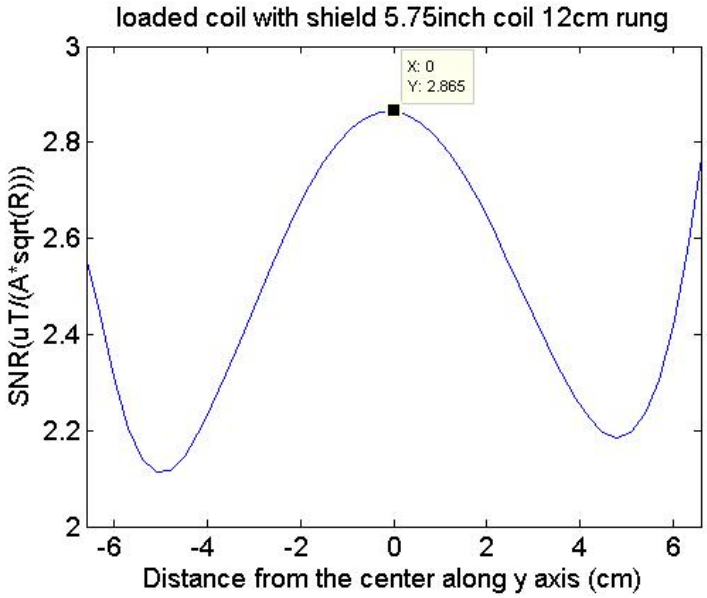

Figure 9 B1 field distribution along the y axis for the modeled 14.6cm coil. The homogenous region along the y axis is 4.4cm, along the x axis is 4.4cm and along the z axis is 3.8cm.

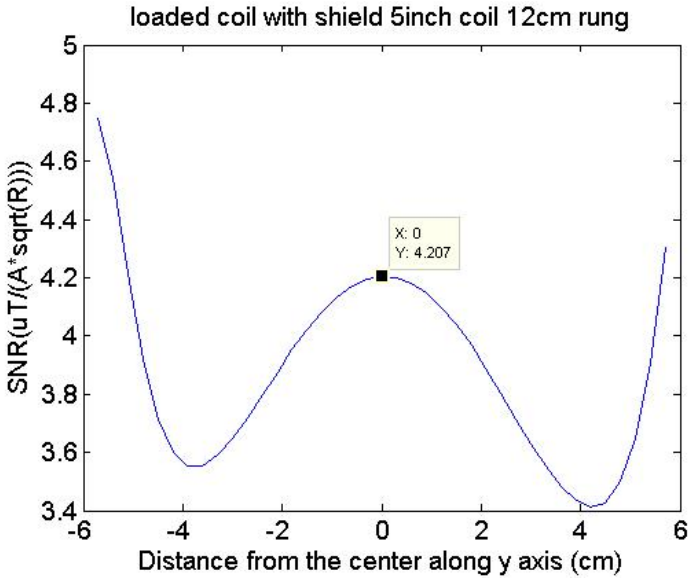

Figure 10 B1 field distribution along the y axis for the modeled 12.7 coil. The homogenous region along the y axis is 4.4cm, along the x axis is 4.4cm and along the z axis is 3.6cm.

Thus, the unshielded coil has a higher SNR compared to the shielded coil. . Furthermore, the homogenous region for the 14.6cm and 12.7cm coil is the same but the SNR of the latter is 49% higher compared to the 14.6cm coil. The SNR of the 12.7cm coil is close the SNR of the unshielded 14.6cm coil. The higher SNR for the 12.7cm coil is because it is farther from the shield compared to the 14.6cm coil.

In conclusion modeling the birdcage coil in FDTD is useful as this gives the researcher an idea on the dimensions to be used for fabricating a coil. In this study only the coil diameter was varied from 12.7cm to 14.6cm but in the future the length of the rung can also be varied from 10.2cm to 25.4cm. From the two coils modeled it can be interpolated that the coil homogeneity is probably going to be same for the coils with diameter anywhere between 12.7cm to 15.4cm. Thus, coil homogeneity can be excluded from consideration and the decision to pick the optimal coil diameter solely depends on the coil SNR and the intended application of the coil. Again, for this study it was considered that the loss in SNR between the 12.7cm and 15.4cm coil was not to significant and thus the 15.4cm coil was chosen given that a surface coil of 13cm diameter had to be inserted in the birdcage coil.

3.3 PIN Diodes

The Birdcage coil was designed so that it can be used as transmit/receive or transmit-only (22). This is accomplished using fast switching PIN diodes (Microsemi Devices, UM9415). When the birdcage coil is used for transmit-only a surface coil is used for received. Both the surface coil and birdcage coil are tuned to the resonant frequency; however when the birdcage coil is transmitting the surface coil is detuned and when the

surface coil is receiving the birdcage coil is detuned. A coil is detuned when the diode is forward biased. A diode driver circuit supplies 150mA and 5V to forward bias the diodes and -13V to reverse bias the diodes. The driver circuit is controlled by the GE Omega System. The bias from the diode driver circuit is carried by parallel twisted pair of wires to the diodes. Along with the diodes, RF chokes are used to isolate the bias voltage from the RF current path (23). The series combination of diode, inductor, variable capacitor and end ring capacitor are used to achieve resonance in the loop (see Fig. 11). All the electronics are mounted on a PCB fabricated and designed in-house and are placed across the end ring capacitors on the birdcage coil. It was found that for all the 3 drives just two diode circuits are sufficient to detune the birdcage coil. These two diode circuits can either be placed across capacitors C7 and C15 in the top end ring or across capacitors C1 and C5 in the bottom end ring. In the past researchers have placed diodes at the feed point; thus they can be placed at C1 and C5 in the bottom end ring (10).

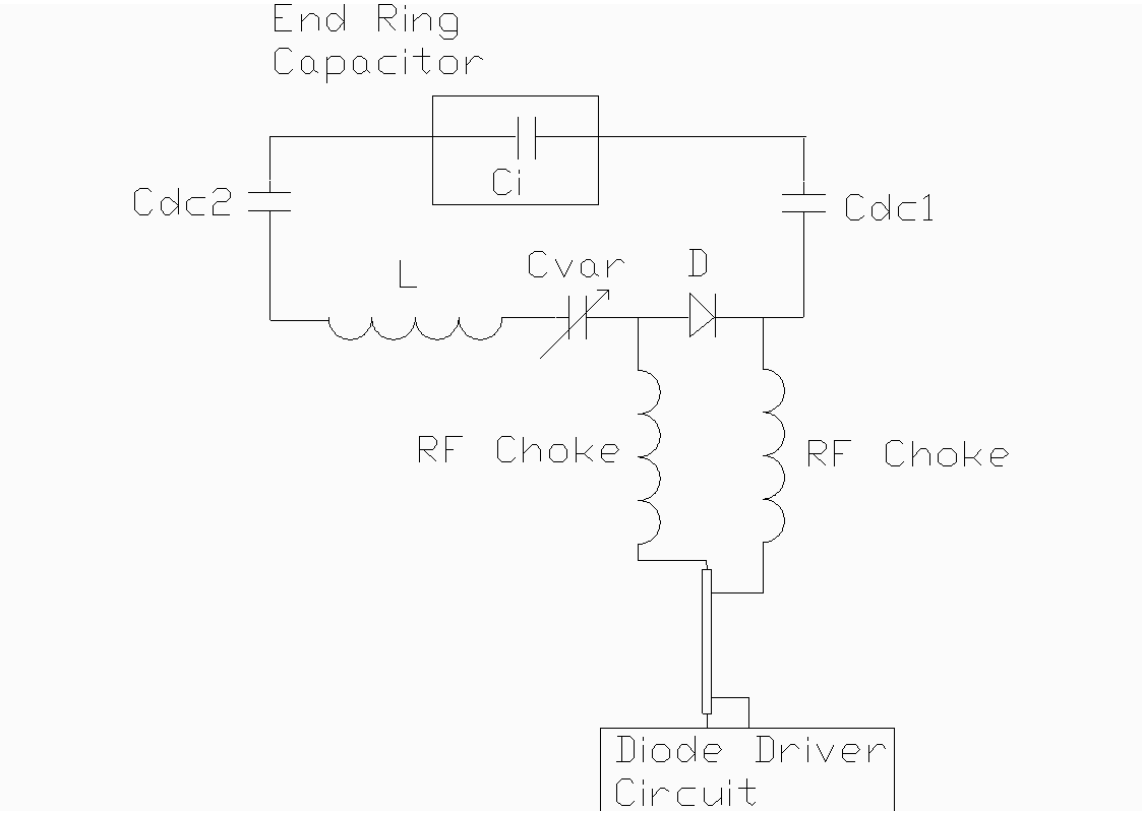

Figure 11 Circuit used for detuning the birdcage coil. In the figure, D is the diode, Cvar is the variable capacitor between 1-20pF, L is 53.5nH (Coil Craft Inductors, 132-04), Cdc1 and Cdc2 are 1 μ F DC block capacitors and Ci is an end ring capacitor on the birdcage coil.

3.4 Surface Coil for Receive

A standard single loop (11,22) surface coil was fabricated for receive. The diameter of the surface coil was 12.7cm. A PIN diode circuit was placed cross C4 (see Fig. 12). The coil was matched to 50ohms by the combination of C1 (ATC, 100B), Cm2 (1-20pF) and Cm1 (1-20pF) variable capacitors. It was tuned to the resonant frequency by trying different value of capacitors at C3 and C5.

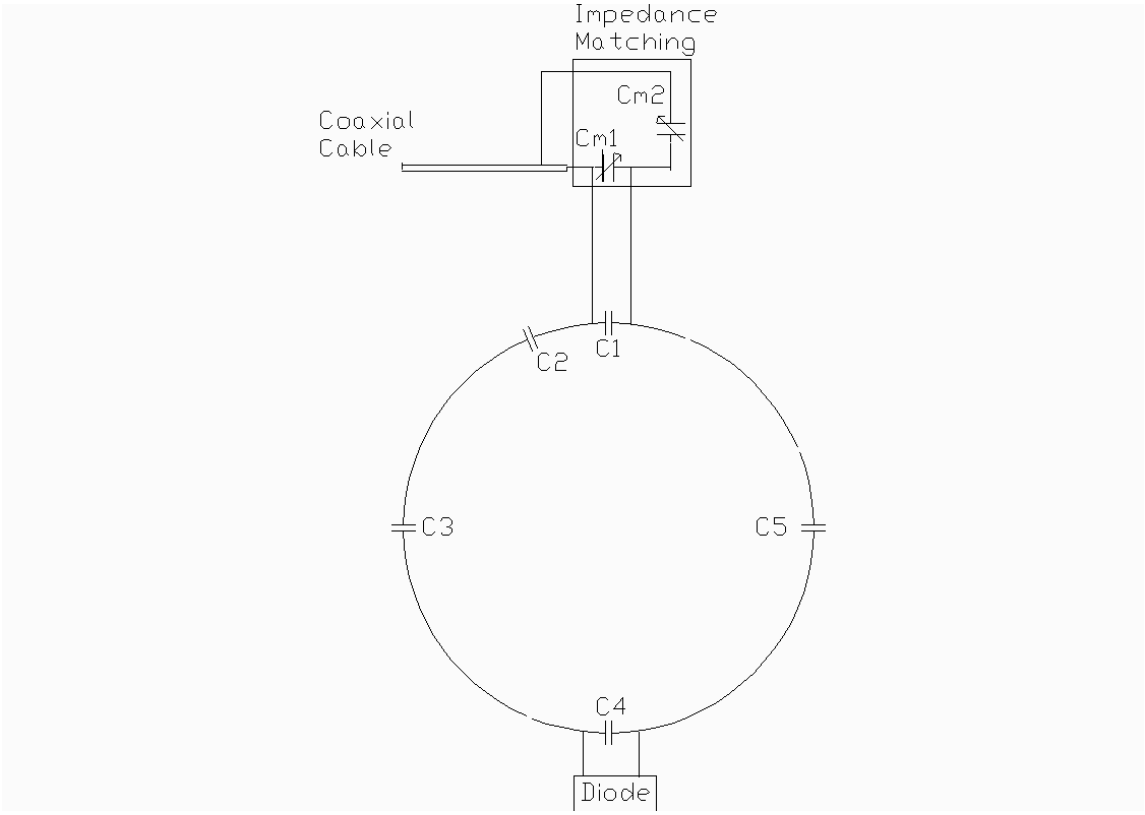

Figure 12 Single loop surface coil for receive. A PIN diode circuit (see Fig. 5) is placed across C3 to detune the surface coil when the birdcage coil is transmitting.

3.5 Tuning

The loaded birdcage coil with the external shield was tuned to 200.237MHz (4.7T/33cm Bruker/GE Omega system). The initial estimate on the end ring capacitor value was provided by BirdcageBuilder (24). For the given coil dimensions the software gave 20pF as the end ring capacitance. When 32 of these capacitors were placed on the end rings the dominant mode (25) of the coil was at 225MHz. The dominant mode of the unloaded coil was tuned to the resonant frequency by viewing S21 and matched to 50ohms by viewing S11 on the HP4195 Network Analyzer. For the S21 measurement Port 1 of the analyzer is connected to the input of the coil and Port 2 of the analyzer is

connected to a pick-up coil. A birdcage coil has (N+2)/2 modes (26), with N being the number of legs. Thus the coil presented has 8 modes, to distinguish the dominant mode from the rest a pick-up coil is moved along the central transverse plane. Since a birdcage coil produces a highly homogenous field at the center of the coil (6), when the pick-up coil is moved in the central transverse plane the mode that shows little variation of the received signal is the dominant mode. Once the frequency at which dominant mode occurs is determined the coil is brought to resonant frequency by changing all 32 end ring capacitors to a value higher or lower depending on the location of the dominant mode. Since, there will be between 1-2MHz shift in resonant frequency of the coil when it is inserted in the magnet due to the gradient coil shield, it is desirable to perform the fine-tuning by changing the length of the rungs. Once the coil is fine-tuned the discontinuity between the two nested tubes is soldered. For this particular coil and shield dimension it was found that the dominant mode is at resonant frequency (204.437MHz) when both the top and bottom end ring capacitors are 25pF.

3.6 Linear Feed

In this drive, the RF power is supplied to the birdcage coil via a balun and T/R switch. A balun is required to eliminate currents flowing on the outside of the 50Ω cables connected to the coil (27). The operation of the T/R switch is controlled by the GE Omega system. Power can be inductively coupled (8, 28) or capacitively coupled (29, 10) to the end ring capacitors. In our design, the power is capacitively coupled (see Fig. 13) via variable capacitors Cm1 and Cm2. These two capacitors are also used to fine-tune the coil to the resonant frequency and match the coil to 50Ω.

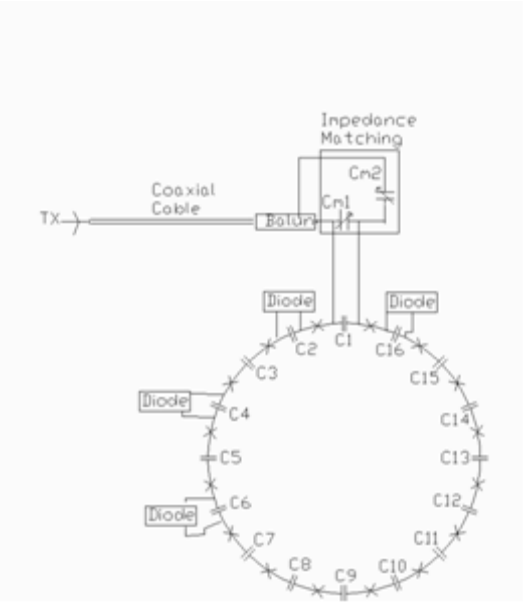

Figure 13 Linear feed. The "Diode" circuit is shown in Figure 5. The circle represents the top end ring of the coil. The X's on the ring are rungs. Cm1 and Cm2 are impedance matching capacitors. The T/R switch and preamp are in the "magnet-leg" of the Varian scanner

3.7 2-port Feed

In a 2-port drive, during transmit two equal amplitude RF signals that are 90^0 out of phase are fed across two top end ring capacitors that are spatially separated by 90^0. During receive; the signals are still 90^0 out of phase but the phase of the received signals is reversed (30). The above can be implemented by using a single quad hybrid (31, 29) or appropriate length transmission lines (4). In this study a single quad hybrid is used (see Fig. 14). The output of the hybrid is connected to C1 (Port 1) and C5 (Port 2) on the top end ring. These 2 feeds will produce two orthogonal resonant modes. Theoretically, the two orthogonal modes should be degenerate however due to non-

uniform reactance at the two ports the modes are usually at different frequencies. Fig. 15 shows the two port feed implemented on the fabricated birdcage coil.

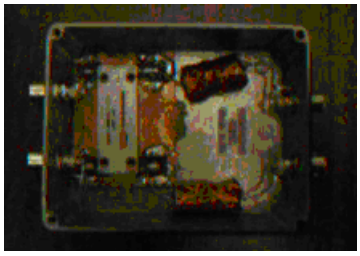

Figure 14 Quad hybrid used along with two baluns on the output of hybrid. The output of the hybrid with the baluns was fed to the two orthogonal coil locations.

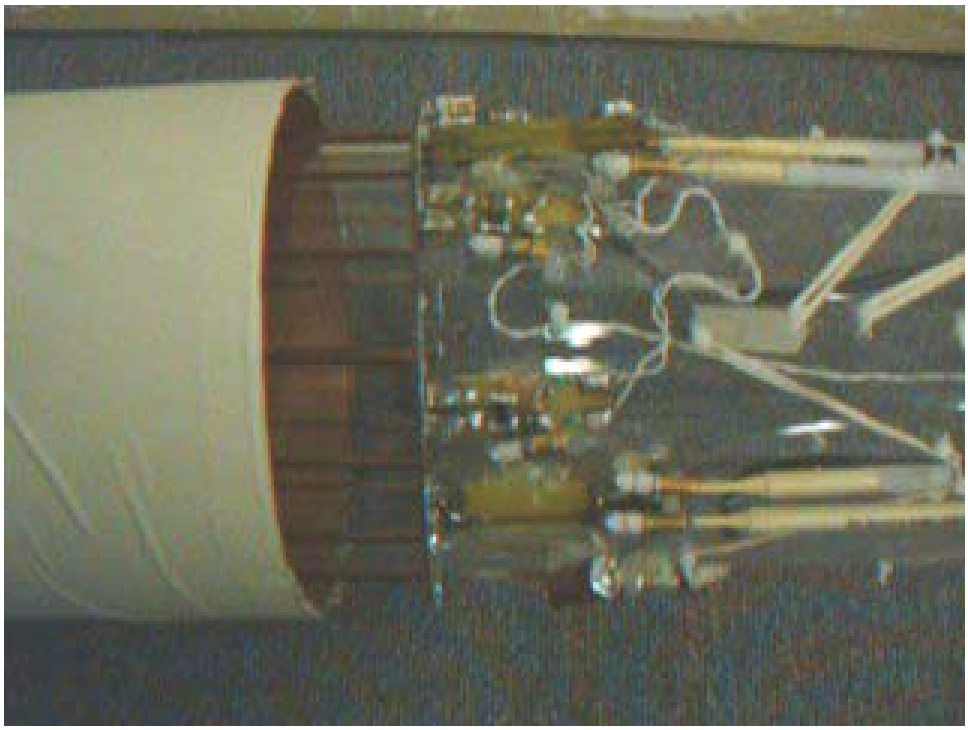

Figure 15 The quadrature drive implemented on the shielded birdcage coil. The coil was fed through a balun and matching/tuning circuit. There were 4 tuning sticks interfacing the match/tune circuit. The twisted pair of wires supply the DC to the diodes required for detuning the coil.

It was found that using the combination of a series and parallel capacitor for matching the coil to 50ohms did not work. The best that the coil could be matched was 23ohms. This could be because of low coil Q. Different capacitor perturbations were tried and it was finally found that by reducing the capacitance from 25pF to 15pF at C9 and C13 top and bottom end ring; I was able to match the coil to 50ohms. There was no measurable loss in SNR or degradation in homogenous region when this capacitor perturbation was made. This has been explained in the patent by Wicherin (32) that the capacitors diagonally opposite from the feed points should be reduced to half their value so as to obtain a "balanced" quadrature drive.

In this study, the two orthogonal modes of the coil was made degenerate by increasing the capacitance at the location (top and bottom) that is diagonally opposite from the feed point. For instance, in the coil presented the two orthogonal resonant modes were at 203MHz (feed C1) and 208.5MHz (feed C5). The resonant mode at 208.5MHz was brought to 203MHz by adding variable capacitors across C13 top and bottom end ring. The isolation when both modes are at same frequency is -4dB, thus the modes need to be isolated. To isolate the two modes capacitance was added across all capacitors except C1, C5, C9 and C13. The value of the capacitor was randomly picked. For this particular asymmetric coil presented a fixed capacitor of 22pF at C14 (top and bottom end ring) was found to give an unloaded coil isolation of -19dB and loaded coil isolation of -18dB. Thus, loading the coil did not bring about a major reduction in isolation. This small loss in isolation by loading a coil is consistent with that reported by Matson (31).

After the two ports on the coil are tuned, matched and isolated the two coil ports are connected to the two ports of the quad hybrid (see Fig. 16). Baluns are placed before the matching circuit and they are also placed at the 4 terminals of the quad hybrid. The transmit port of the hybrid is connected to the "transmit" connector on the magnet leg and the receive port of the hybrid is connected to the "preamp in" connector on the magnet leg.

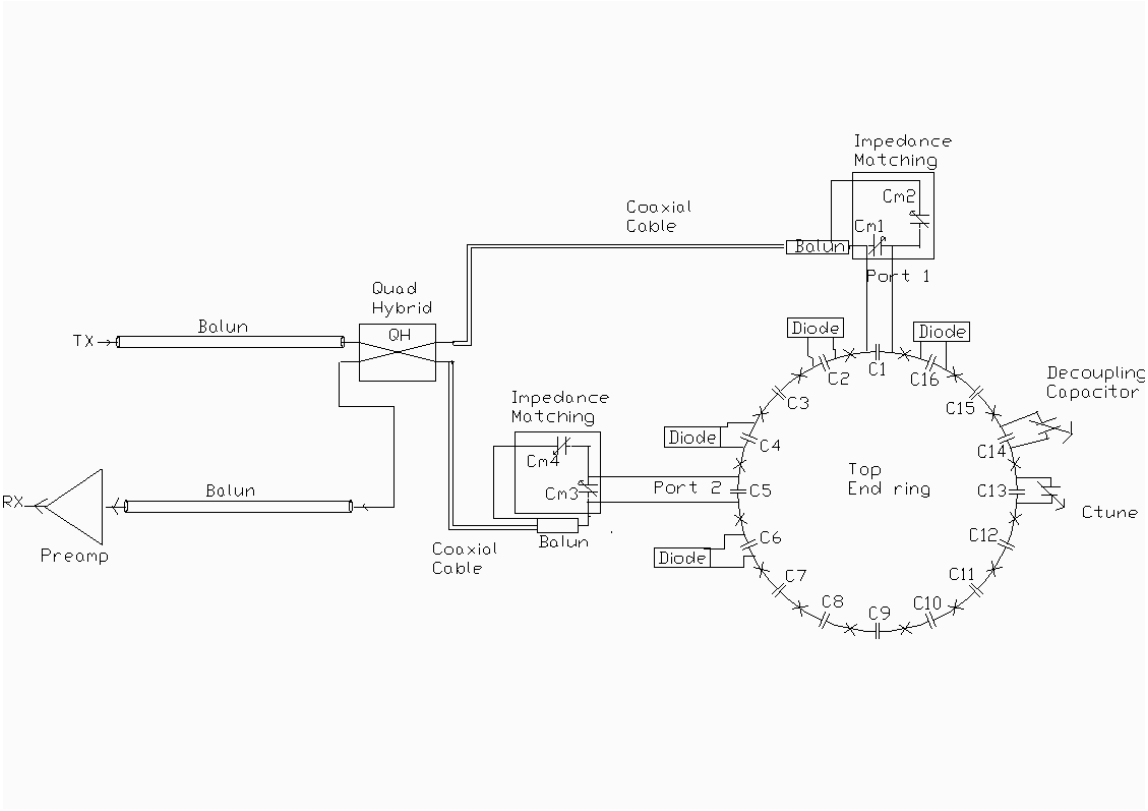

Figure 16 2-port feed. The PIN diode circuit (see Fig. 1) is placed across C2, C4, C6 and C16. A fixed decoupling capacitor is used to isolate the two modes. This capacitor is placed across C14. A fixed capacitor is also placed across C13 to bring the two orthogonal resonant modes to the same frequency. QH is the quad hybrid that feeds the two ports across capacitors C1 (Port 1) and C5 (Port 2). The coaxial cables are λ/2 long.

3.8 4-port Feed

The 4-port presented was implemented but it did not work. This is because due to the sinusoidal current distribution on the rungs it is not possible to isolate the two feeds that are diagonally opposite from each other. It is not possible for a high-pass coil but it may work for a band-stop coil.

The 4-port drive involves feeding 4 equal amplitude RF signals with fixed phases 0^0, 90^0, 180^0 and 270^0 across 4 top end ring capacitors that are spatially separated by 90^0. This drive has been implemented in the past either by using a 90^0 hybrid and two $\lambda/2$ coaxial cables on a birdcage coil (33) or a combination of 90^0 hybrids and 180^0 combiners on a TEM coil (34,11). The former approach was not preferred by us as each of the outputs of the quad hybrid is fed to two ports of the coil. The power feeding the 2 ports will be equal only if the impedance of the two ports is equal. This equal impedance at the 2 ports of the coil can be difficult to achieve due to human errors in the fabrication of the coil. Also, debugging this drive is difficult as one cannot individually monitor the return loss of each of the ports once the quad hybrid is connected. Lastly, the 4-port TEM coil approach was also not implanted by us as it required 180^0 combiners; these combiners were not available off the shelf. In this study a slight variation of the former approach was implemented. The variation is that the 4 outputs of the 2-stage hybrid are connected to 4 ports of the coil. A 2-stage quad hybrid design is presented with a 180^0 phase shifter on one of the ports (see Fig. 17). A fixed $\lambda/2$ length coaxial cable is used to achieve the 180^0 phase shift. Once each of the 4-ports

are matched to 50ohms the 4 outputs of the 2-stage quad hybrids are connected to the coil with λ/2 length coaxial cables. When fine-tuning and matching the ports it is important to verify that the birdcage is at the dominant mode for each of the ports. Similar to the 2-port feed, no trimmer capacitors are used to improve the isolation between the four ports instead the coil geometry is relied on to give the best possible isolation between each of the ports.

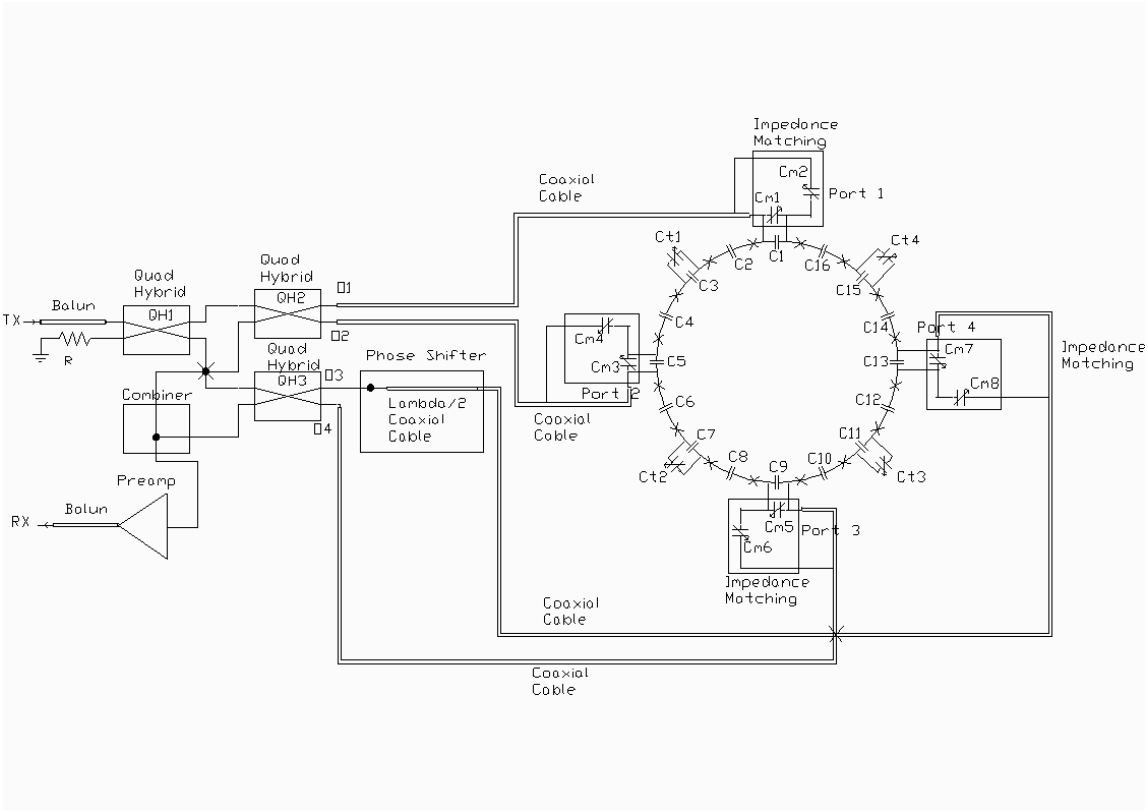

Figure 17 4-port feed. The PIN diode circuit (see Fig. 1) is placed across C2 and C16 (not shown in this figure). The output of the quad hybrids QH2 and QH3 feed the four ports- C1 (Port 1), C5 (Port 2), C9 (Port 3) and C13 (Port 4). The outputs O1, O2, O3 and O4 have phase 0^0, 90^0, 90^0 and 180^0 with respect to O1. Thus a 180 phase shifter is required at O3. λ/2 length coaxial cables connect the quad hybrid to the 4 ports. Also, the cables between the 2 stages of hybrid are λ/2 long to maintain the phase difference.

4. RESULTS

The performance of the loaded and unloaded fabricated birdcage coil was tested. The bench test included measurement of the Q factor, B1 field mapping of the central transverse plane for the unloaded coil, SNR, current distribution, shift in resonant frequency due to shield and effect of having a transmit-only/receive only coil as opposed to a transmit/receive coil. Images of the saline, oil and CuSO4 phantoms were taken for the 1-port feed. The performance of this coil was compared to the performance of two other birdcage coils both on bench and by taking images. Lastly, images were taken of a saline phantom and oil for 2-port feed.

A S21 measurement was performed to evaluate the Q factor of the coil. The channel 1 of network analyzer was connected to one of the ports of the birdcage coil and channel 2 of the analyzer was connected to a pick-up coil. The pick-up coil was placed at the center of the coil. Before performing the S21 measurement the feed port of the coil was matched to 50ohms. The ratio of the Q factor of the unloaded (Q= 50) over loaded coil (Q=16) was 3.1. A ratio of 5 is usually considered to be excellent (5). The loaded Q is always lower in magnitude than the unloaded coil Q because when the coil is loaded with a sample the sample losses dominate and thus it reduces the energy being stored in free space. Hence the loaded coil Q is lower than unloaded coil Q. The unloaded Q of the coil depends on the Q of inductors and capacitors as their respective losses are comparable. The loaded coil Q is what we would expect, however the unloaded Q for the coil presented is lower than expected. The unloaded Q can be increased when the rung width is increased, coil length is shortened and the number of

rungs is decreased. Doty (5) experimentally evaluated the unloaded Q and loaded Q of various birdcage coils and explained their relation to coils with different length, rung width, rungs, coil and shield diameter.

Similar to the Q factor measurement, the B1 field in the central transverse plane is mapped with a pick-up probe. For the 2-port feed the channel 1 of the analyzer is connected to the input of the quad hybrid and channel 2 of the analyzer was connected to the pick-up probe. The pick-up probe was moved at increments of 3mm across the x and y axis of the unloaded coil (35). Fig. 18 & Fig. 19(z axis) shows that the homogenous region (the region where the B1 amplitude is within 10% of the maximum central B1 value) of the fabricated coil is 9.4cm, 14.5cm and 15cm along the x, y and z axis respectively. The cylindrical region where the B1 field is within 10% of the maximum B1 field is $1041cm^3$, the total volume of the FOV of the birdcage coil is $3350cm^3$. Thus, the ratio of homogenous region to the total FOV of the coil is 31%.

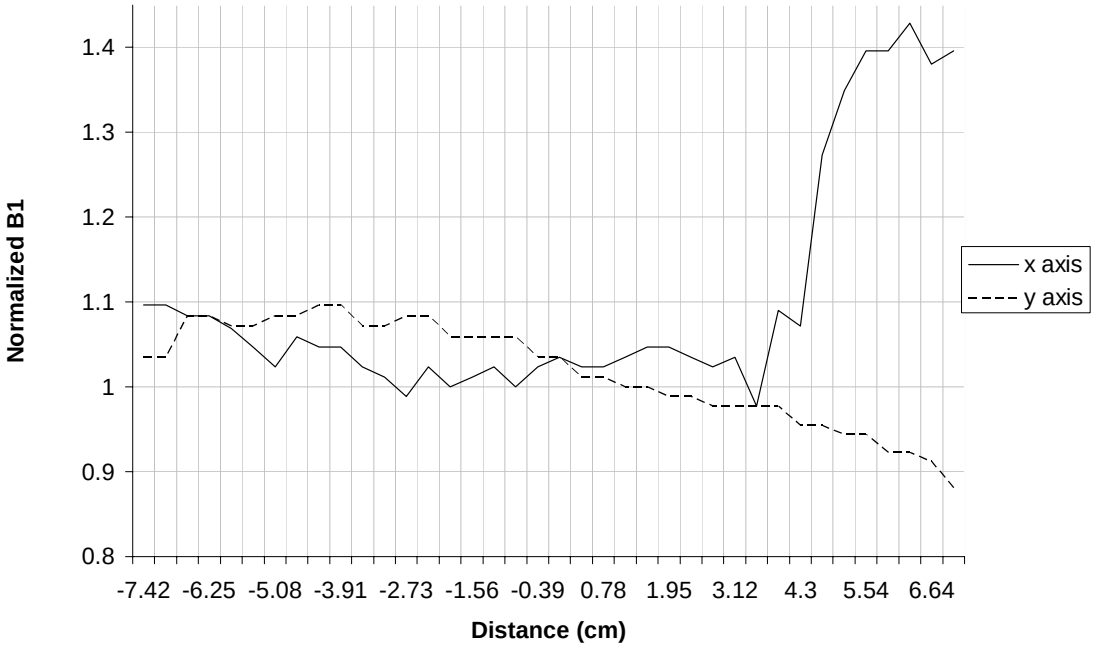

Figure 18 B1 field distribution for the linear drive along the x and y axis. The probe was moved in the central transverse plane in increments of 3mm. This shows that the coil is on the dominant mode as the B1 field is uniform.

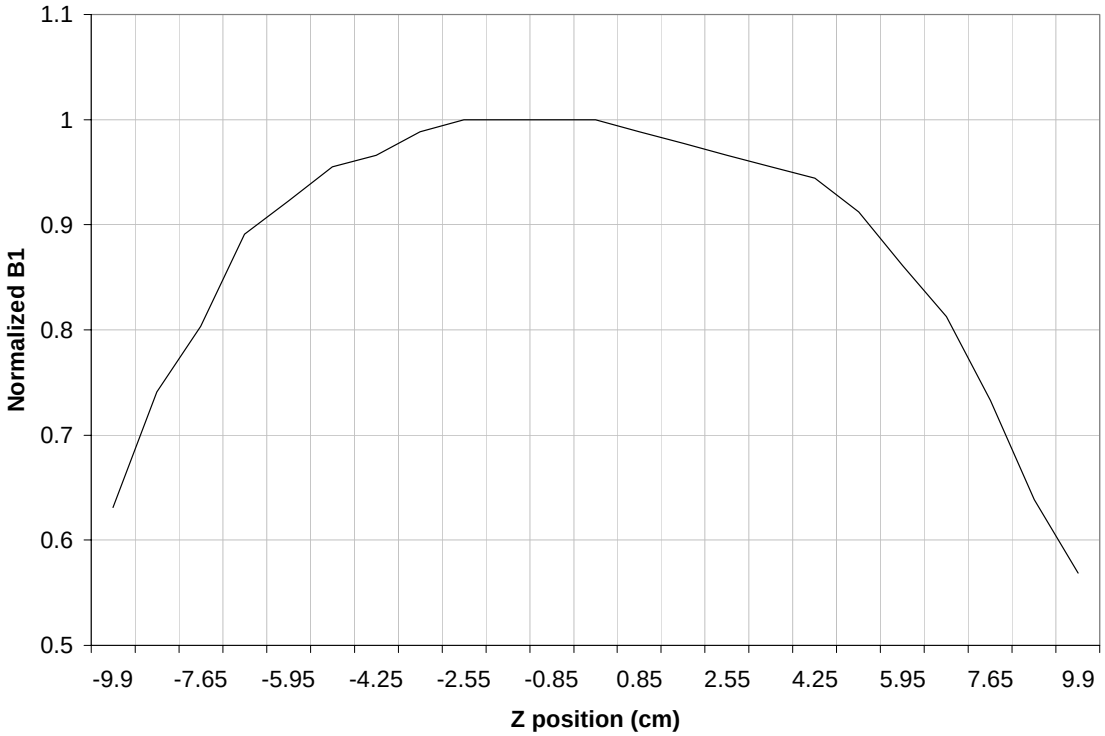

Figure 19 B1 field distribution for the linear drive along the z axis. The probe was moved along the z axis and along the centre of the coil. The B1 field is maximum at the center and is minimum at the two end rings.

Table2 Comparison of SNR and homogeneity on the bench of the coil presented and two other coils currently in the lab. The SNR measurement was performed for a loaded coil, but the homogeneity measurement is for an unloaded coil.

Type of feed	Type of Birdcage Coil	Normalized SNR	ΔX (cm)	ΔY (cm)
1-port	Cu tube-15.5cm coil	1	9.4	13.8
2-port	Cu tube-15.5cm coil	1.33	n. a	n. a
1-port	Cu tape-15.5cm coil	0.67	10.6	6
1-port	trombone-10cm coil	2.4	4	9.8

Table 2 compares the homogeneity of the coil presented ("Cu tube-15.5cm" coil) to 'Cu tape-15.5cm" coil and "trombone-10cm" coil. The coil dimensions of "Cu tape-15.5cm" coil were rung length=25cm, coil diameter=15.5cm and shield diameter=17.7cm. The coil dimensions of "trombone-10cm" were rung length=20cm, coil diameter=10cm and the coil was unshielded. The table shows that the homogenous region of the "Cu tape-15.5cm" coil (see Fig. 20) was 37% lower than the "Cu tube-15.5cm" coil. Similarly the homogeneous region of the "trombone-10cm" coil (see Fig. 21) was 48% lower than the "Cu tube-15.5cm" coil.

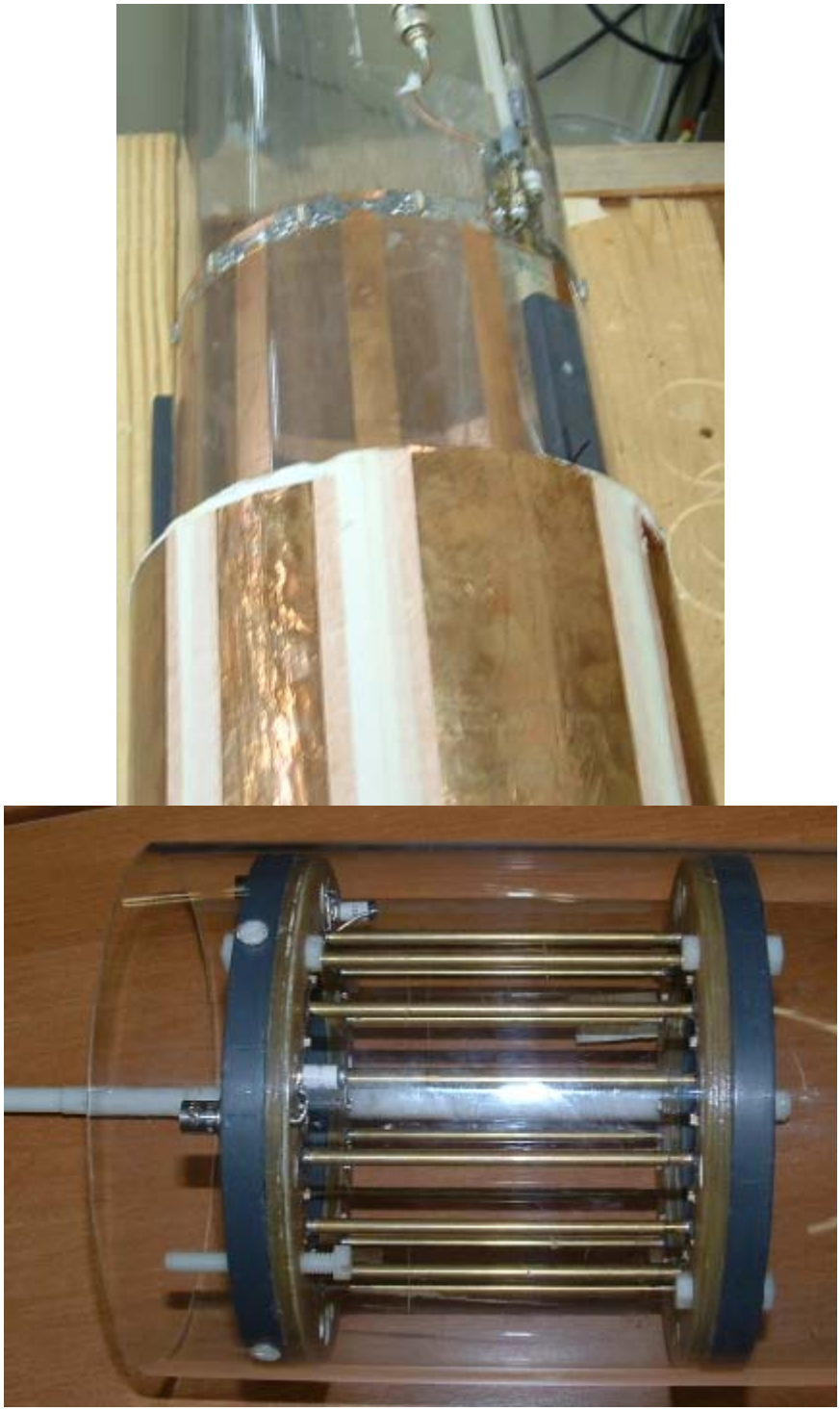

Figure 20 Top is a picture of the “Cu tape-15.5cm” coil and bottom is the “trombone-10cm” unshielded coil. The coil length is 25cm, coil diameter is 15.5cm, shield diameter is 17.2cm of the former coil and coil length is 15cm and coil diameter is 10cm of the “trombone-10cm” coil.

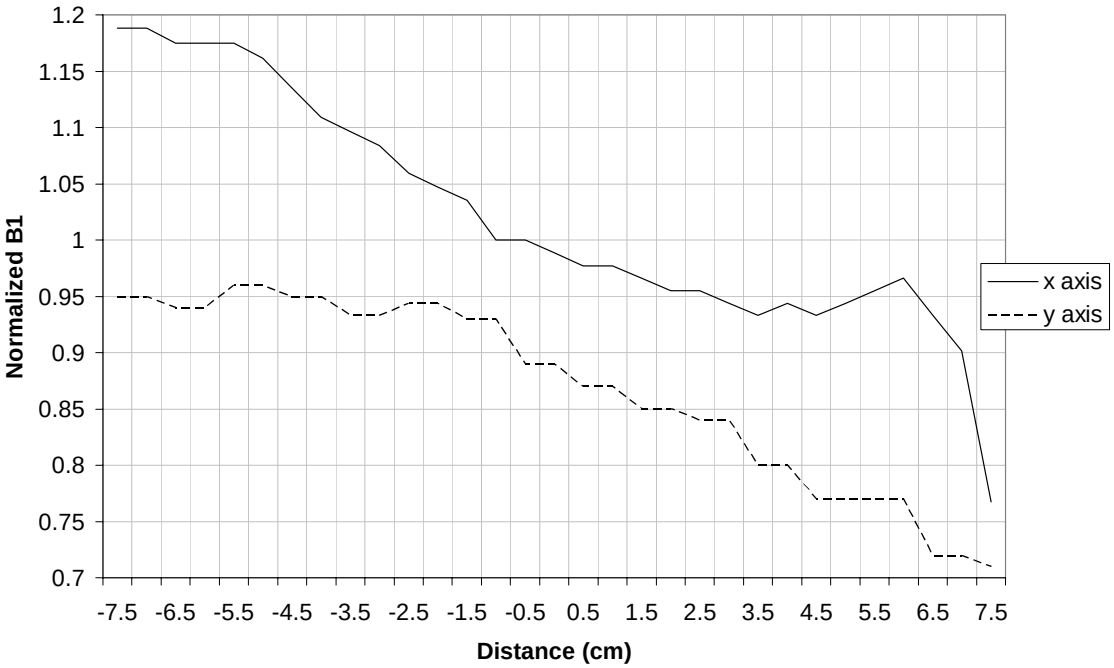

Figure 21 Homogeneity along x and y axis of "Cu tape-14.6cm" coil. This plot shows that the circular homogenous region is 6cm. The coil presented is the same dimension as "Cu tape-14.6cm" but has a greater homogeneity region (9.4cm). The region of the coil presented is bigger by 37%.

The homogeneity measurement made for the "Cu tape-15.5cm" coil is shown in Fig. 22. The homogeneous region of the coil presented in thesis is bigger than the former coil.

The homogeneity along the x axis is smaller compared to y axis because the coil is being fed along the x axis. This is because the magnetic flux lines are stronger close to the feed and also because when the probe is close to the rungs it excites the birdcage coil. The homogeneity along the z axis is a hump with a maximum at the center and minimum close to the end rings because a standing wave is created in the rungs. The

rungs are $\lambda/8$ in length. By making the rungs longer the difference between the peak magnetic field at the center and at the two edges will be higher.

It was not possible to make a reliable homogeneity measurement for the 2-port feed for an unloaded coil. This is because the isolation between the two ports as seen through the quad hybrid fluctuates when the coil is loaded due to the proximity of my hand and coil. Thus, to observe the homogeneity of the 2-port drive it is necessary to image the coil with an oil phantom (low dielectric constant). A phantom dielectric constant that is close to the air dielectric constant would mean that the standing wave effect would be absent. Therefore, the oil phantom is equivalent to an unloaded coil.

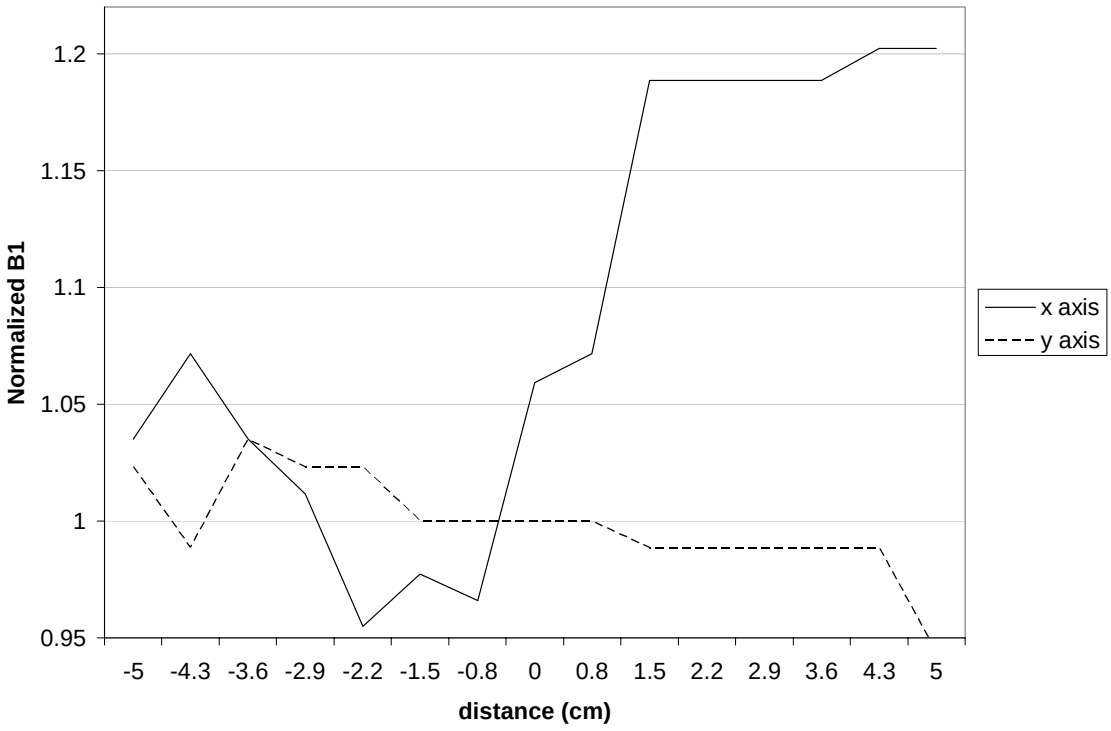

Figure 22 Homogeneity measurement along x and y axis for the "trombone-10cm coil". The circular region of homogeneity was 2cm. The coil presented has a homogenous region that is 58% higher than the "trombone-10cm coil".

Additionally the SNR at the center of the birdcage coil was measured using a single pick-up probe and a crossed pick-up probe (see Fig. 23). The formula used to calculate SNR; $\frac{B1}{\sqrt{R}}$ (15). In this equation B1 is the signal received by the Analyzer and R is the resistance of the coil at the feed point. Table 2 states the SNR of the 3 birdcage coils; “Cu tube-15.5cm” (coil presented in this thesis), “Cu tape-15.5cm” and “trombone-10cm”. It can be seen that the smaller coil “trombone-10cm” has a 140% higher SNR compared “Cu tube-15.5cm”. The higher SNR of the 10cm coil with respect to the 15.5cm coil was unexpected. The “Cu tube-15.5cm” has a 33% higher SNR compared to a similar dimension “Cu tape-15.5cm”. Also, the 2-port drive implemented on the “Cu tube-15.5cm” shows a 33% improvement in SNR.

Figure 23 Probe used for the homogeneity measurements for all 3 coils. This probe was commercially obtained.

Furthermore the dominant mode of the birdcage coil shifts 2MHz lower when the coil is loaded with a cylindrical saline phantom. It shifts lower because loading a coil increase the total resistance. The total resistance as in the eq 2.25 above is composed of the resistance of coil, resistance of sample and resistance of shield. Thus, inserting a

sample into the coil increases the total resistance and thus the dominant mode shifts lower.

The birdcage coil was also tested in the transmit-only mode by inserting a surface coil in the FOV of the birdcage. It was seen that the isolation between the transmit port of the birdcage and receive port of the surface coil -23.2dB. It was found that when the birdcage coil is detuned the dominant mode of the coil shifts to a higher frequency. This makes sense because when the diode is forward biased the series combination of the capacitor on the diode circuit and the end-ring capacitor will give a lower capacitance than the actual end ring capacitor. Specifically, the end ring capacitance is 25pF and the series capacitor on the diode circuit is 10pF; the series combination of these capacitors will give 7pF which is lower than the rest of the 25pF end ring capacitors. Lowering the capacitance at any of the ports is equivalent to increasing the resonant frequency ($w = \frac{1}{\sqrt{LC}}$). Furthermore, it was found that there was no measurable change in SNR and homogeneity by inserting these diodes. This finding is consistent with that reported by Barberi (22). One would expect there to be some loss in coil SNR when diodes are inserted as opposed a coil without diodes because there will some leakage current through the diodes. This leakage DC current will add to the RF current on the end-ring and thus degrade the SNR. However, the diode circuit design presented in this work and that by Barberi used two DC blocking capacitors to stop the DC current from reaching the end rings.

The crossed pick-up probe (see Fig. 1) was also used to verify circular polarization for the 2-port. As mentioned previously, circular polarization is achieved when the two modes are at the resonant frequency amplitude of the 2 modes are equal and are 90^{o} out of phase. To verify circular polarization, the change in amplitude and phase of the 2 modes is recoded as the crossed probe placed at the center is rotated by 360^{o} (see Fig. 24 & Fig. 25) If circular polarization is achieved then the level of RF detected on a pick-up loop remained independent of pick-up loop orientation (31).

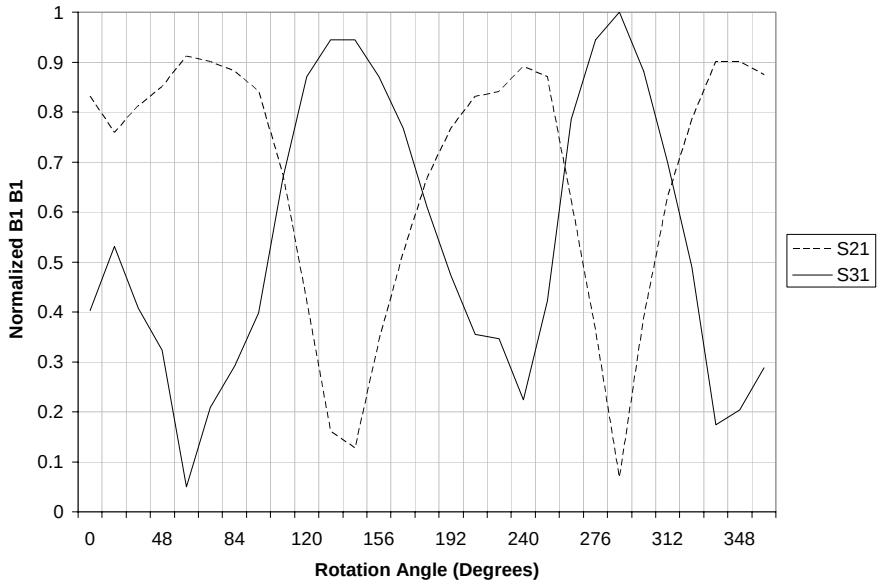

Figure 24 Amplitude of the orthogonal dominant mode of the loaded coil for 1-port feed. The crossed pick-up probe was placed at the center of the coil and rotated 360^{0} in increments of 5^{0}. It can be seen that the coil is receiving only Bx or By field at any given time. This shows that the coil is linearly polarized.

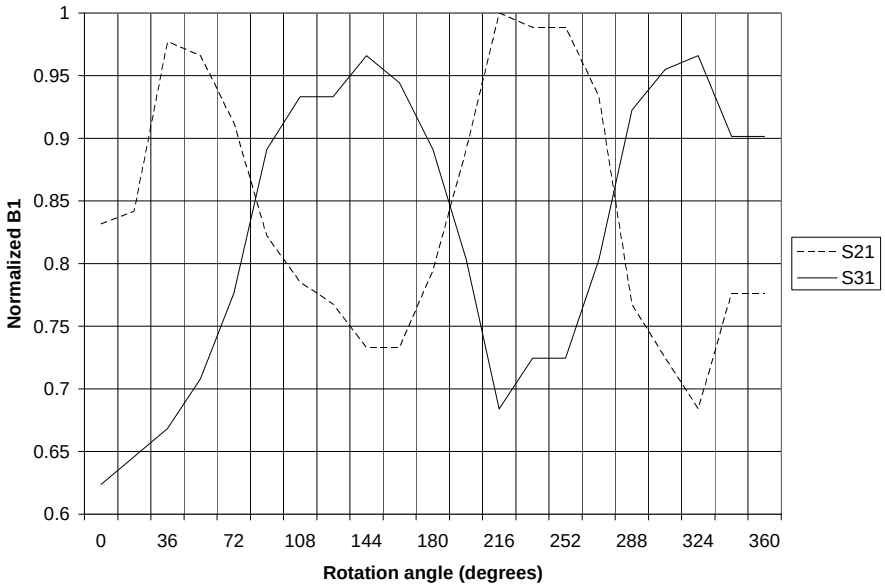

Figure 25 Amplitude of the two orthogonal resonant modes of the loaded birdcage coil with 2-port feed. The crossed pick-up probe was placed at the center of the coil and rotated 360^0 in increments of 5^0 At 144degrees the amplitude difference between the two modes is 0.3 in linear scale. The equivalent of 0.3 in linear scale is 3dB in log scale. These two orthogonal modes when passed through a receive quad hybrid should show constant amplitude.

Lastly, the current distribution was measured by placing planar pair coils adjacent to each of the 16 rungs. This was done to observe the improvement in distribution when the coil is fed with 3 different power drives. In the past current distribution was measured by placing a small sense loop on each of the rungs (36). A planar pair coil is preferred over a single loop coil because of the localized field sensitivity and low coupling with the nearest neighbor coil (18). The planar pair coil fabricated was 2cm long, 0.8cm wide and 0.2cm trace widths. Equal length coaxial cables connected the planar pair coils to the network analyzer for a S21 measurement.

Fig. 26 compares the current distribution of a high-pass coil modeled by Ibrahim (37) in FDTD and the measured distribution on the Cu tube-15.5cm coil. It can be seen

that the two distributions are not sinusoid. The shape and amplitude of the two distributions are similar between rung 6 to 9. Between rungs 1 to 5 the shape is similar but the amplitude is not the same. Thus, it can be seen that the strategy to compare the improvement in current distribution from 1-port, 2-port to 4-port is not valid.

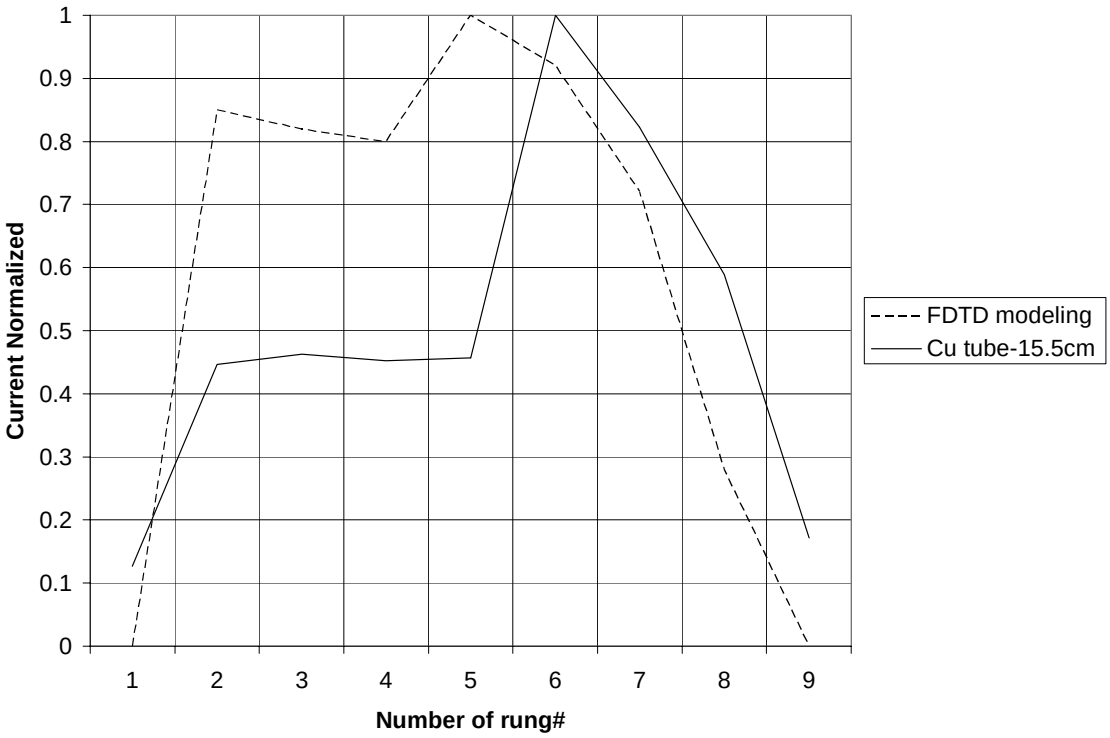

Figure 26 Current distribution on the rungs was measured using 16 planar pair coils. The current on the fabricated coil is compared with that obtained by FDTD modeling (37). It can be seen that both distributions deviate from the ideal sinusoid.

5. DISCUSSION

The aim of this thesis was to fabricate a mechanically rigid birdcage coil and then implement an optimized 2-port drive. Typically for any new coil design it is modeled in a software like HFSS or XFDTD. The advantage of modeling a coil first is that one can visualize the field patterns for the particular coil geometry, make capacitor perturbations on the modeled coil and observe the changes in homogeneity, SNR and Q. An attempt was made to model the coil in FDTD but the results generated were not reliable. Thus, we decided to pick the coil diameter so that the single-echo-acquisition (SEA) coil can be inserted in the FOV of the birdcage coil. To use the SEA coil for receive it is necessary to detune the birdcage coil; to make this possible diodes are used on the birdcage coil and surface coil. Once the coil diameter was fixed the coil had to be shielded due to high-field coil radiation losses. These radiation losses will degrade the coil SNR. The biggest shield that could be used was the size of the bore. It turned out that the shield diameter was only 4cm larger than the coil diameter. Theoretically, a coil that is far away from the sample the coil will have higher homogeneity and lower SNR compared to the case where the coil is closer to the sample. Inserting a closely spaced shield on a large coil will further degrade the coil SNR and homogeneity. Again, modeling is the best approach to numerically characterizing the SNR and homogeneity.

To fabricate a mechanically rigid coil we decided to use Cu tubes, FR-4 end rings, tuning sticks with dials and mount matching/tuning/diode on rectangular FR-4 pieces. After fabrication the coil was tuned to resonant frequency by placing fixed high Q capacitors at different places on the coil. The coil was fine tuned to resonant

frequency by altering the length of the rungs. This had to be done due to variability in the shift of the resonant frequency of the coil when inserted in the magnet and to account for the shift in resonant frequency after making the required capacitor perturbations to achieve an isolated/tuned/matched 2-port drive. The matching of the linear drive did not require any capacitor to be perturbed. However, to correct for the asymmetry in the 2-port coil; a capacitor had to be placed diagonally opposite from the feed point with the higher self-resonant frequency to equal the lower self-resonant frequency of the other feed point. Next, matching the two ports to 50ohms required that the capacitor diagonally opposite the two feed points be halved in relation to all the other end ring capacitors. Lastly, to isolate the two orthogonal modes a fixed capacitor (22pF) was used at a particular location on the top and bottom end ring to achieve an unloaded isolation of -19dB and loaded isolation of -18dB.

An attempt was made to implement the four port drive. However, isolating the four ports of the coil using the presented high-pass coil did not work. Theoretically, this is because the current distribution in the rungs is a sinusoidal which means that the rungs that are right next to the two feeds that are 180degrees apart have high current amplitude. Thus, using 4 decoupling capacitors at 45degree locations to the feeds will not work. The two designs that might work is to create a band-stop coil or to tune the two feeds that are 180degrees apart through a quad hybrid. The latter case of tuning 4-port coils was adopted by Vaughan (11), the isolation seen by the quad hybrid will be -20dB or better, however in reality the two feeds are not isolated.

Measurements were made on the bench to measure the Q, SNR and homogeneity of the coil presented and two other coils that are currently in the lab. The unloaded Q of the coil presented was lower than expected. As explained by Doty (5) that unloaded coil Q can be increased by using high Q capacitors, high Q inductors and decreasing the number of rungs. Again, modeling is the best approach to obtain the desired loaded and unloaded Q by optimizing the coil design. Next, homogeneity measurements were made on bench in the linear mode for all 3 coils. The measurements show that the homogenous region (B1 variation within $\pm$ 10% of the maximum central B1 value) for the coil presented is 37% higher than the "Cu tape-15.5cm" coil and homogenous region of coil presented is 48% higher than the unshielded "trombone-10cm" coil. Thus, the homogeneity of the coil presented is better than the other two coils in the lab. The above finding is consistent and has been theoretically explained in the above paragraph. However, the SNR of the "trombone-10cm" coil presented is 140% higher than the coil presented. This large difference in SNR was unpredicted. However, it is difficult to say as to why the "trombone-10cm" coil has such a higher SNR. It could be because it is unshielded or because it is small. The coil presented has a volume (FOV) of 3773.83cm^3 but the trombone coil has a volume of 1178.09cm^3. Thus, in terms of volume the coil presented is 3.2 times bigger than the trombone coil. But the coil presented has 37% higher coil SNR compared to "Cu tape-15.5cm". This could be because the coil is only 2cm away from the shield, whereas the coil presented is 4cm away from the shield. There are 16 diodes placed on the bottom end ring, it is possible that those diodes is

reducing the SNR. For the coil presented it was found that 4 diodes were sufficient to detune the birdcage coil and there was no measurable change in SNR and homogeneity.

Lastly, to make the tuning/matching of the coil easy for the user; four tuning sticks were mounted on the 4 variable capacitors. Dials were also mounted on the ends of the tuning stick. The dials were used to keep track of the position of the variable capacitor. For commonly used phantoms the position of the dials were documented. Thus, tuning/matching of the two ports of the birdcage coil is made easy for the user.

5.1 Birdcage Coil Fabrication Issues

The following is a list of issues about coil design that I had faced during my work. For the next coil that I would build I would consider these factors into my design.

a) Coil asymmetry: A coil is asymmetric when the fabricated coil structure deviates from the ideal birdcage coil structure. According to the ideal birdcage coil structure all the rungs should be equal length, all capacitors on the end ring should be equal value, all capacitors and rungs should be equidistant from each other, absence of matching/tuning loops and a perfectly symmetrically positioned shield. The coil that I fabricated was asymmetric firstly because the rungs were not equal length. The Cu tubes obtained from the manufacture were 12” in length; since the coil was supposed to be only 6” (152.3mm) in length- the Cu tubes had to be cut. The variation between the 16 tubes that were used for my design was 0.039” (1mm). The variation of 0.039” gives rise to variation in the phase of the current in the meshes. Thus each mesh in-turn produces different B1 fields leading to B1 field inhomogeneity. Also, different length tube means

that the inductance of the two tubes that make a mesh is unequal. If the inductance of a leg is unequal from the rest of the legs then the capacitor needed to resonate this mesh will be unequal from the rest of the end ring capacitors. Next time a machine/ factory should be used/ asked to cut 6" tubes for us. Secondly, the capacitors used in this design had a tolerance $\pm 5\%$. Again, if the capacitance of each of the capacitors on the end ring is unequal the resonant frequencies of each of the meshes will be different. We decided to pursue with the tolerance $\pm 5\%$ capacitors as opposed to tolerance $\pm 2\%$ capacitors as the latter capacitors are double the price of the former. Specifically, the price of a non-magnetic 100B series ATC capacitor with tolerance $\pm 5\%$ is $2.8 per capacitor and the price of tolerance $\pm 2\%$ is $4.5 per capacitor. Thus, after performing a cost-benefit analysis we concluded that we will purchase the tolerance $\pm 5\%$ capacitor. Thirdly, in my design the LPKF prototyper was used to make 16 equidistant holes to insert the tubes and solder them to the end rings. However, I did not use the LPKF to make 32 equidistant slots on the end rings for the capacitors to be soldered. I used an exacto knife to make the slots. Thus all 32 slots neither equidistant from each other nor do they have the same width. The width of the slot can be thought of as a capacitor too. In retrospect, the LPKF/PROTEL should have been used to make the slots so that they are equal in width and equidistant from each other. It is slightly more work to make these slots in PROTEL but it will reduce the asymmetry of the coil. Fourthly, the L-network comprising of series and parallel capacitors used on the coil to

accomplish matching and tuning gives rise to coil asymmetry. It was found that as expected the series matching capacitor did not change the self-resonant frequency of the coil and so does not lead to coil asymmetry. However, the parallel tuning capacitor does change the current distribution leading to coil asymmetry. In the desired application of the coil it was necessary that the coil be made tunable for different loads thus a tuning capacitor is necessary; this tuning cap leads to some asymmetry that is unavoidable. Lastly, the placement of shield also leads to coil asymmetry. While wrapping the shield on a former; a smooth former should be selected and the shield should be in close contact to the former i.e. eliminate pockets of air/ vacuum between the shield and former. Sometimes to the naked eye it looks like the shield is in close contact to the former; a good test to solve this confusion is to rotate the coil inside the shield. If the dominant mode of the coil splits or shifts away from the tuned resonant frequency -this is probably because either the shield is not long enough or because the shield is not symmetric about the coil. The symmetry of the shield about the coil axis becomes important for coils that are closely spaced to the shield.

b) Strategy to make the coil symmetric/ Cap perturbations: As I had mentioned in the previous paragraph that there are various sources that make the coil asymmetric. It is difficult to narrow down as to which source creates the greatest asymmetry. Thus, it is difficult to say what can be done to make the coil symmetric. However, I would like to suggest a few correction strategies that can be implemented that I tried. The following commentary is in reference to Fig. 8

that shows the two feeds and numbers the capacitor. The two things to remember while making cap perturbations is that; firstly at any given point the same capacitance should be added at the top and bottom end rings and the same capacitance should be added 180^{o} away from the place where the cap perturbation was made. For instance, if the user would like to improve the isolation between the two feed points C1 and C5; and the effectiveness of the point C3 is to be tested in improving the isolation. Then a capacitor smaller than 33pF should be soldered at C3 on the top end ring and C3 on the bottom end ring, also the same capacitance should be soldered 180^{o} apart from C3 that is C11 in the top and bottom end ring. Adding a cap perturbation more than 33pF at any point reduces the homogeneity/SNR of the coil. The above mentioned cap perturbation at C3 and C11 might work for some coil but for the asymmetric coil that I had built this did not work. For my coil, I found that adding capacitance (22pF) at C3 top and bottom end rings lowers the isolation by about 2dB. Next, I found that adding capacitance (22pF) only at C11 top and bottom gives me an isolation of -22dB unloaded coil and -18dB for the loaded coil. But the capacitance of 22pF at C11 works when the match/tune networks at the two feeds are disconnected from the coil and the coil is directly excited by the analyzer. When the match/tune network and the balun were added the location of C11 did not isolate the coil. Various values from 1pF to 33pF were tried and I found that 22pF gives the best isolation at C11. For the configuration when the match/tune network is connected to the coil the same 22pF was soldered at different points

on the top and bottom end ring. It was found that there are 3 locations on the coil (C14, C15 and C7) that will give an isolation of -19dB for unloaded coil and -18dB for loaded coil. All locations other than C1, C5, C3, C11, C7, C14 and C15 caused the dominant mode of the coil to split. The dominant mode of the coil should not split because this will reduce the homogeneity of the coil. In conclusion, when the parallel tuning capacitor at the two feeds is used to bring the coil to 200MHz, this reduces the isolation between the two ports. The isolation can be improved by adding a correction capacitor at one of the remaining 14 locations. Once the coil is isolated on the bench with a particular capacitor, that capacitor need not be changed once the coil is in the magnet. The isolation will get better when it is inserted in the magnet.

c) Strip-line quad hybrid: The decision to buy a commercial strip-line quad hybrid paid-off in terms of stability, low insertion loss (0.3dB), narrow band and compact non-magnetic package that can be placed half wavelength away from the two feeds. The quad hybrid was a sample given by Innovative Power Products (IPP) to us. In retrospect, we should have purchased the quad hybrid from IPP with BNC connectors mounted on the hybrid. This would have improved the performance of the hybrid. In the design presented the strip-line hybrid had to be mounted on a rectangular PCB and then 4 female BNC connectors were soldered on the PCB. It is this mismatch between the strips of the hybrid and the BNC connector that causes the output to be -3.6dB and -3.2dB instead of both being -3dB. Also, the phase difference between the two outputs

of the hybrid presented over here is 84^{o} but it should be exactly 90^{o}. Thus, a quad hybrid with BNC connectors should be purchased. I believe the BNC connector hybrids from IPP are custom made with a lead time of 8 weeks and they are priced at $250 a piece.

d) Balun: Balun is required to eliminate currents flowing on the outer shield of the cables and also to eliminate instability of S parameter measurements. In the absence of balun the measured S parameter depends on the placement of cables and by touching the cables the S parameters change. In the lab, conventionally we have used cylindrical balun and ferrite rings. A cylindrical balun is where a few turns (inductor) of coaxial cable are placed inside shielded cylindrical plastic tubing and a capacitor is placed in parallel to the inductor to achieve resonance. The cylindrical balun is narrow band in the sense that the impedance is high (Z>1000ohms) only for a range of 1MHz. This narrow band makes the inductor difficult to resonate as we are limited by fixed value ATC caps. We would like to use ATC caps instead of variable capacitors as the Q of the ATC caps is high. If the Q of the inductor and capacitor is high then this will help get a higher impedance (>3000ohms). This narrow band range is acceptable for the scanner/magnet experiment since the bandwidth of the RF pulse is a few KHz. However for bench tuning of the coil there can be a shift in frequency of about 1-5MHz from 200MHz due to asymmetric shield, asymmetric coil, loading of birdcage and asymmetric cap perturbations. One approach to solve this problem would be to use different cylindrical balun for different frequency. But this

approach would require the user to make a large number of cylindrical balun and this is not feasible. Thus, for bench tuning RF coils it is necessary to use a wide-band balun. A wide-band balun can be made using circular ferrite rings. This is made when a few turns of the cable are wound over the ferrite ring. Even though ferrite rings are somewhat effective in reducing the problems mentioned above; they cannot be inserted in the magnet and thus a coil tuned on the bench using ferrite rings is not necessarily going to perform the same when it is inserted in the magnet with a cylindrical balun. In conclusion, to ensure that there is a one is to one correlation between a coil tuned on the bench and the coil in the magnet- a bazooka balun should be used. A tri-axial cable is used to fabricate a bazooka balun (tri-axial cable is where there are two outer shields and an inner conductor, a co-axial cable is where there is only one shield and an inner conductor). The two outer shields are shorted by using a pin. It has been used by Matson (31) for their dual-tuned birdcage coil. The bazooka balun will be wide-band and can be used for bench and magnet coil tuning.

e) Trombone design: For good homogeneity and to maintain the natural sinusoidal current distribution it is important that the parallel tuning capacitor for the two feeds be kept to a minimum. So we should make sure that the self- resonant frequency of the coil (no match/tune loops) be as close to 200.228MHz as possible both in the magnet and on the bench. The self- resonant frequency will be different in the magnet than on the bench. For instance, if the self-resonant frequency of coil is tuned at 200.228MHz on the bench then in the magnet it will

be anywhere from 200MHz to 202MHz. Thus, to account for this shift in resonant frequency the trombone design is useful. The overlap between the nested rungs can be increased/ decreased to bring it back to 200.228MHz. The trombone design works well for linear feed coils. However for 2-port coils where the self-resonant frequencies of both meshes need to be at 200.228MHz the trombone design fails for asymmetric coils.

f) Location of match/ tune network: 3 different positions of match/tune network were investigated. The first location was where the match/tune was on the coil, the second location was where a short piece of coaxial cable was placed between the match/tune network and the coil, the third location was where one wavelength (105cm) long cable was placed between the coil and the match/tune network. The theory behind the location of match/tune network is that the coil Q will be lower the farther the match/tune network is placed from the coil. This theory was true for the last case where the matching circuit was placed one wavelength cable away from the coil. It was found that the loaded Q of the coil stayed the same at 21, however the unloaded Q decreased from 60 to 45. The decrease in unloaded Q was more than 10% and this was unacceptable. The motivation of placing the matching circuit a wavelength away from the coil was that this would eliminate the need for long tuning sticks. Since the aim of the project was to make the coil robust, there was a mechanical point of failure and that was the fail-proof mounting of the tuning stick on the small screw of the Voltronics variable capacitor. This idea was abandoned because coil performance

could not be sacrificed for mechanical reasons. Furthermore, when the matching circuit was placed on the coil I was not able to get S11 to -20dB or match the coil to 50ohms. I was only able to match it to 23ohms. This is probably because of low coil Q. Thus, I decided to move the matching circuit 10cm away from the coil by using a 10cm length cable. In this configuration I was able to match the coil to 50ohms. Care should be taken that the length of the cable between coil and matching circuit should be less than $1/10^{th}$ of a wavelength. (I have no journal article to cite this fact but it is a rule of thumb followed by the industry.) A cable longer than $1/10^{th}$ would I believe again reduce the unloaded coil Q.

g) Variable capacitor with shaft: As mentioned in the above section titled "Location of match/tune network" the mechanical stability of placing a small screw driver at the end of tuning sticks on a 0.3cm diameter screw is an issue. An alternate to mounting screw driver at the end of tuning sticks would be to purchase a variable capacitor with a shaft (see Fig. 27). The tuning stick can be glued to the large surface area of the shaft. The cost of the non-magnetic variable capacitor with a screw from Voltronics is $120 with a lead time of 4 weeks. The cost of adding a shaft to the variable capacitor is an additional $5.

Figure 27 The cap on the right is currently used on the coil. A tuning stick with a small screw driver has to be mounted on this capacitor. The diameter of this screw is 0.3cm. The mechanical stability of this tuning stick on a small surface area (0.3cm) is an area of concern. Thus, we should use the capacitor on the left with a shaft on the capacitor. The advantage of the shaft is that it does not need a small screw driver at the end of the tuning stick. The tuning stick can be glued to the large surface area of the shaft.

h) Measurement of current distribution: The current distribution was measured by placing small 16 planar pair coils on the rungs of the birdcage coil. This was done to see the improvement in the sinusoidal current distribution as we go from 1-port to 2-port to 4-port. Even though the distribution measured on the bench was not sinusoid but it is similar to the distribution shown by FDTD modeling by Ibrahim (referenced earlier). In retrospect if I was going to redo the measurement of the current on the legs I would make a few changes to the experimental setup. Firstly, cut equal length cables so that the phase and amplitude of the S21 (received signal) can be mapped. Recording the phase and amplitude will give us the sinusoidal distribution where there is a positive peak and a negative peak. Secondly, 16 baluns should be placed on each of the 16

planar pair coils to make the measurement stable and reliable. However fabricating 16 cylindrical balun is time consuming and so I would propose that the experimenter use a "bazooka" balun. Thirdly, all 16 planar pair coils should be directly connected to the 64 channel network analyzer. This will measure the distribution all at the same time. By measuring S21 one at a time by connecting the network analyzer to each of the planar pair coils introduces errors. There will be errors as the received signal is sensitive to the orientation of the coil in the shield. The coil/ shield should not be rotated or moved while making the measurement. When the network analyzer is individually connected to each of the 16 coils; the movement of coil/shield is inevitable.

i) Gradient coil simulator: It is general knowledge that a coil tuned on the bench should be when inserted in the magnet be tunable. But there a few issues of integrating a big volume coil in a small bore magnet which the coil designer should keep in mind while designing coils. There are changes in the self-resonant frequency of the two ports of the coil and the isolation between the two ports when the coil is inserted in the magnet. Again because of the asymmetry in the placement of the RF coil in the magnet the two ports of the coil will shift differently. The shifting of self-resonant frequency of the coil when inserted in the magnet is not an issue for a single port but it becomes an issue for two port drives. It's not an issue for a single port drive as the parallel tuning capacitor can be tweaked to bring the coil back to resonance at 200MHz. However, for the 2-port isolation scheme proposed over here it is important that the self-resonant

frequency of both ports of the coil is the same without using any tuning capacitor at the two feed points. Secondly, it was noticed that the isolation between the 2-ports usually improves when the coil is inserted in the magnet between 2 to 4dB. This improvement of isolation in the magnet means that a longer RF shield should have been used. The current RF shield was twice the length of the coil. I guess a RF shield 3 times the length of the coil should have been designed. In conclusion, I would like to propose that in the future a person tuning birdcage coils on the bench should first build a gradient coil simulator. The goal of the simulator would be to deign and build a gradient shield equivalent on the bench so that when the RF coil is inserted in the magnet without the gradient simulator there would be no change in isolation or shifting of the self-resonant frequency of the coil.

j) End-cap: This is a feature that can be added to the coil design to improve the B1 field homogeneity near the end-capped region. It improves near the end-capped region as it reduces the B field produced by the end ring currents. These end ring currents serve to destroy the B1 field homogeneity along the z axis. The end cap is a circular conductive sheet that is placed at one end of the coil. The conducting sheet acts like a mirror for the coil and effectively doubles it electrical length. It was decided that this feature will not be added to the coil as it will force the entry of the phantom of the coil in only one direction.

6. CONCLUSION

A quadrature birdcage coil was successfully fabricated and tested on the bench. On the bench there is a 30% improvement in SNR of the quadrature coil compared to the linear coil. The improvement in homogeneity and the RF transmission power of a quadrature coil over the linear coil will be investigated by taking spin-echo images. Also, the ability of the coil presented to achieve circular polarization amongst different coil loadings will be investigated. Furthermore, it was shown that the fabricated coil in the linear mode has a SNR that is 30% higher than a similar dimension ("Cu tape-14.6cm") birdcage coil.

REFERENCES

1. Edelstein WA, Schenck JF, Mueller OM, Hayes CE. 1987. Radio frequency field coil for NMR. U.S. patent 4 680 548.
2. Wang J, Yang QX, Zhang X, Collins CM, Smith MB, Zhu XH, Adriany G, Ugurbil K, Chen W. 2002. Polarization of the RF field in a human head at high field: a study with a quadrature surface coil at 7.0 T. Magn Reson Med 48(2):362-369.
3. Chen CN, Hoult DI, Sank VJ. 1983. Quadrarue detection coil - a further square-root 2 improvement in sensitivity. J Magn Reson 54:324-327.
4. Eash MG. 1989. Apparatus for tuning an NMR field coil. U.S. patent 4 820 985.
5. Doty FD, Entzminger G, Hauck CD, Staab JP. 1999. Practical aspects of birdcage coils. J Magn Reson 138(1):144-54.
6. Ibrahim TS, Lee R, Baertlein BA, Robitaille PM. 2001. B1 field homogeneity and SAR calculations for the birdcage coil. Phys Med Biol 46(2):609-19.
7. Ibrahim TS, Lee R, Baertlein BA, Kangarlu A, Robitaille PL. 2000. Application of finite difference time domain method for the design of birdcage RF head coils using multi-port excitations. Magn Reson Imaging 18(6):733-42.
8. Dardzinski BJ, Li S, Collins CM, Williams GD, Smith MB. 1998. A birdcage coil tuned by RF shielding for application at 9.4 T. J Magn Reson 131(1):32-8.

9. McDougall MP, Brown DG, Spence D, Wright SM. 2001. A low-pass trombone birdcage coil with broad tuning range. Proc 9th Annual Meeting ISMRM, Glasgow, Scotland, UK. p 1256.

10. Lin FH, Kwong KK, Huang IJ, Belliveau JW, Wald LL. 2003. Degenerate mode birdcage volume coil for sensitivity-encoded imaging. Magn Reson Med 50(5):1107-1111.

11. Vaughan JT, Adriany G, Garwood M, Yacoub E, Duong T, DelaBarre L, Andersen P, Ugurbil K. 2002. Detunable transverse electromagnetic(TEM) volume coil for high-field NMR. Magn Reson Med 47(5):990-1000.

12. Jones R. 1995. NMR Quadrature Detection Array. U.S. patent 5 430 378.

13. Matsunaga Y. 1995. Multiple coil adopting a quadrature detection method applied thereto and a signal processing circuit employing the same in an NMR apparatus in a vertical magnetic system. U.S. patent 5 457 386.

14. Duensing G BH, Fitzsimmons JR. 1996. Maximizing SNR in the presence of coil coupling. J Magn Reson 111:230-235.

15. Wright SM, Wald LL. 1997. Theory and application of array coils in MR spectroscopy. NMR Biomed 10(8):394-410.

16. Tropp J. 1990. Method of correcting an asymmetry in an NMR radio frequency coil and an improved radio frequency coil having N-fold symmetry and reduced eddy current. U.S. patent 5 196 797.

17. Bridges JF. 1987. Cavity resonator with improved magnetic field uniformity for high frequency operation and reduced dielectric heating in NMR imaging devices. U.S. patent 4 751 464.

18. McDougall MP, Wright SM. 2005. 64-channel array coil for single echo acquisition magnetic resonance imaging. Magn Reson Med 54:386:392.

19. Spence D. 2005. Master list of general electric magnetic resonance imaging phantoms. Wisconsin: General Electric.

20. Spence DK, Wright SM. 2003. 2-D full wave solution for the analysis and design of birdcage coils. Concepts Magn Reson B (Magn Reson Eng) 18(1):15-23.

21. Collins CM, Smith MB. 2001. Signal-to-noise ratio and absorbed power as functions of main magnetic field strength, and definition of“90°” RF pulse for the head in the birdcage coil. Magn Reson Med 45(4):684-691.

22. Barberi EA, Gati JS, Rutt BK, Menon RS. 2000. A transmit-only/receive-only(TORO) RF system for high-field MRI/MRS applications. Magn Reson Med 43:284-289.

23. Ledden PJ, Wald LL, Hinton DP. 2002. A detunable elliptic transmission line resonator for body imaging at 3 Tesla. Concepts Magn Reson B (Magn Reson Eng) 15(1):92-100.

24. Chin CL, Collins CM, Li S, Dardzinski BJ, Smith MB. 1998. BirdcageBuilder. 1.0: Copyright Center for NMR Research, Department of Radiology, Penn State University College of Medicine.

25. Chen J, Feng Z, Jin JM. 1998. Numerical simulation of SAR and B-field inhomogeneity of shielded RF coils loaded with the human head. IEEE Transactions on Biomedical Engineering 45(5):650-659.

26. Vullo T, Zipagan RT, Pascone R, Whalen JP, Cahill PT. 1992. Experimental design and fabrication of birdcage resonators for magnetic resonance imaging. Magn Reson Med 24(2):243-52.

27. Wright SM. 2002. Full-wave analysis of planar radiofrequency coils and coil arrays with assumed current distribution. Concepts Magn Reson B (Magn Reson Eng) 15:2-14.

28. Murphy-Boesch J, Srinivasan R, Carvajal L, Brown TR. 1994. Two configurations of the four-ring birdcage coil for 1H imaging and 1H-decoupled 31P spectroscopy of the human head. J Magn Reson 103(2):103-14.

29. Vaughan JT, Hetherington HP, Otu JO, Pan JW, Pohost GM. 1994. High frequency volume coils for clinical NMR imaging and spectroscopy. Magn Reson Med 32(2):206-18.

30. Jin J. 1998. Electromagnetic analysis and design in magnetic resonance imaging. Florida: CRC Press.

31. Matson GB, Vermathen P, Hill TC. 1999. A practical double-tuned 1 H/31 P quadrature birdcage headcoil optimized for 31 P operation. Magn Reson Med 42(1):173-182.

32. Wichern AHW, Leussler CG. 1991. MR examination apparatus comprising a circuit for decoupling the two coil systems of a quadrature coil arrangement. U.S patent 4 998 066.

33. Ledden PJ, Wald LL, Vaughan JT. 2000. A four-port drive flat-element transmission-line coil for brain imaging at 3 T. Proc. of the 8th In'tl Soc for Magnetic Resonance in Medicine, Toronto, Canada. p 1395.

34. Vaughan JT, Adriany G, Snyder CJ, Tian J, Thiel T, Bolinger L, Liu H, DelaBarre L, Ugurbil K. 2004. Efficient high-frequency body coil for high-field MRI. Magn Reson Med 52(4):851-9.

35. Tomanek B, Volotovskyy V, Gruwel MLH, McKenzie E, King SB. 2005. Double-Frequency Birdcage Volume Coils for 4.7 T and 7T. Concepts Magn Reson B (Magn Reson Eng) 26(1):16-22.

36. Fitzsimmons JR, Beck BL, Brooker HR. 1993. Double Resonant Quadrature Birdcage. Magn Reson Med 30:107-114.

37. Ibrahim TS, Lee R, Baertlein BA, Y Y, Robitaille PL. 2000. Computational analysis of the high-pass birdcage resonator: finite difference time domain simulations for high-field MRI. Magn Reson Imaging 18:835-843.

VITA

Name:	Vishal Virendra Kampani
Address:	Biomedical Engineering, 337 Zachry Engineering Center, 3120 TAMU, College Station, TX-77843-3120
Email Address:	vishal60@gmail.com
Education:	B.S., Electrical Engineering, University of Illinois-Urbana Champaign, 2005 M.S., Biomedical Engineering, Texas A&M University, 2008